Evolution of Neoarchaean supracrustal belts at the northern margin of the North Atlantic Craton, West Greenland

Julie A. Hollis, Marie Keiding, Bo Møller Stensgaard, Jeroen A.M. van Gool and Adam A. Garde

The Archaean North Atlantic Craton of West Greenland collided at *c.* 1.9 Ga with a lesser-known Archaean craton to the north, to form the Nagssugtoqidian orogen. The Palaeoproterozoic metamorphic grade and strain intensity decrease northward through the orogen, allowing investigation of the reworked Archaean components in its northern part. Two Archaean supracrustal belts in this region – the Ikamiut and Kangilinaaq belts – are investigated here using field mapping, aeromagnetic data, zircon geochronology, and geochemistry. Both belts comprise quartzo-feldspathic and pelitic metasedimentary rocks, amphibolite, and minor calc-silicate rocks, anorthosite and ultramafic rocks. Pb-Pb and U-Pb dating of detrital zircons and host orthogneisses suggest deposition at *c.* 2800 Ma (Kangilinaaq belt) and after 2740 Ma (Ikamiut belt); both belts have zircons with Neoarchaean metamorphic rims. Metasedimentary rocks and orthogneisses at Ikamiut share similar steep REE signatures with strong LREE enrichment, consistent with local derivation of the sediment and deposition directly onto or proximal to the regional orthogneiss precursors. Zircon age data from Kangilinaaq indicate both local and distal sources for the sediment there. Geochemical data for Kangilinaaq amphibolites indicate bimodal, mixed felsic–mafic source rocks with island-arc basaltic affinities, consistent with a shelf or arc setting. Both belts experienced a similar tectono-metamorphic history involving Neoarchaean amphibolite facies peak metamorphism at *c.* 2740–2700 Ma, possibly due to continued emplacement of tonalitic and granodioritic magmas. Nagssugtoqidian lower amphibolite facies metamorphism at *c.* 1850 Ma was associated with development of the large-scale F_2 folds and shear zones that control the present outcrop pattern. The observed differences in the sources of the Kangilinaaq and Ikamiut belts and their shared post-Archaean history suggest they were formed in different Neoarchaean environments proximal to and on a continental plate, and were amalgamated in a convergent margin setting shortly after their deposition.

Keywords: North Atlantic Craton, northern Nagssugtoqidian orogen, LA-ICP-MS, SIMS, zircon

---

J.A.H., B.M.S., J.A.M.v.G. & A.A.G., *Geological Survey of Denmark and Greenland, Øster Voldgade 10, DK-1350 Copenhagen K, Denmark.* E-mail: *jho@geus.dk*
M.K., *Geological Museum, University of Copenhagen, Øster Voldgade 5–7, DK-1350 Copenhagen K, Denmark.*

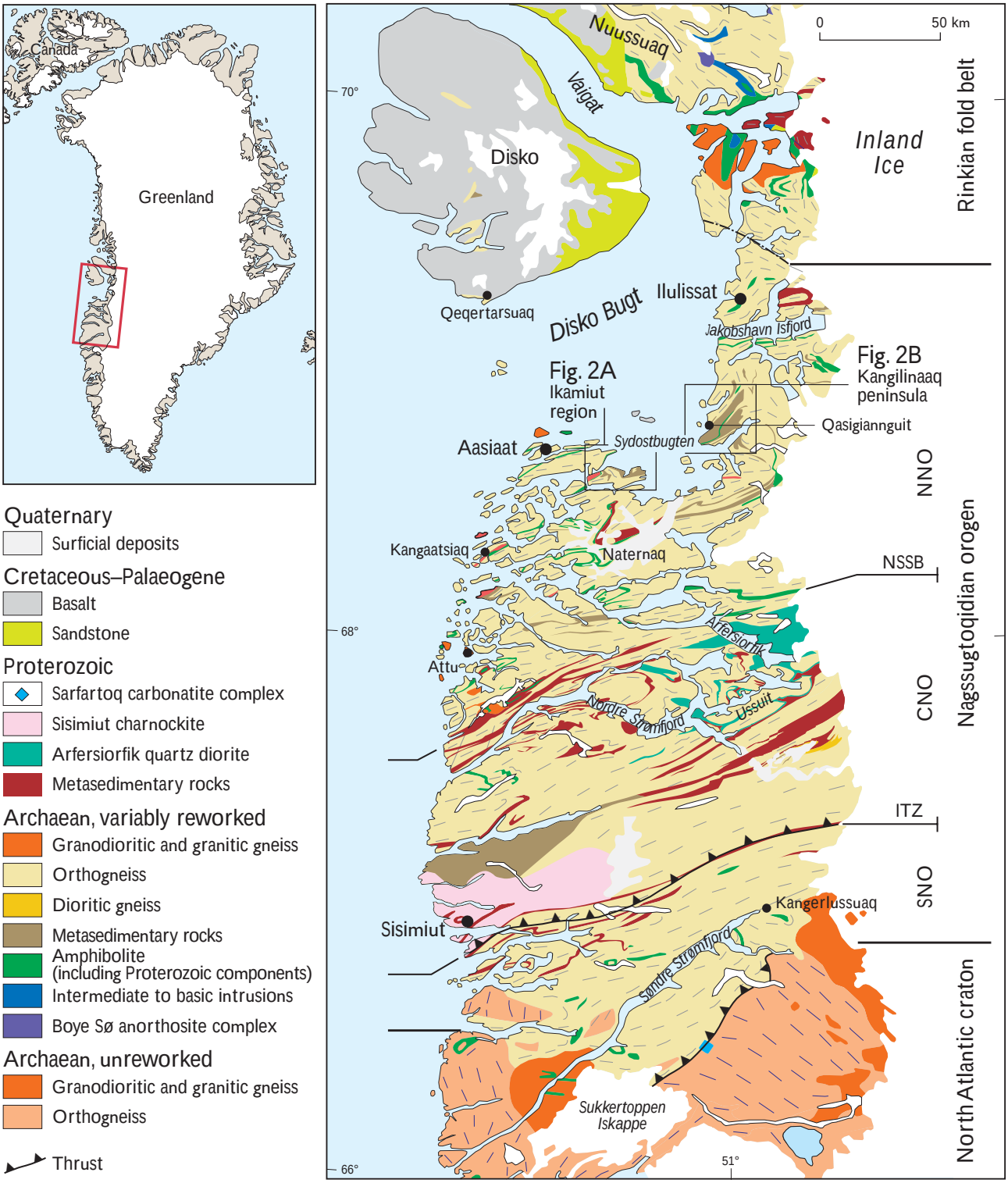

Fig. 1. Geological map of the Nagssugtoqidian orogen, West Greenland, from van Gool *et al.* (2002b). Frames show locations of Figs 2 and 3.

The Palaeoproterozoic Nagssugtoqidian orogen, central West Greenland, comprises Archaean and less abundant Proterozoic orthogneiss and metasedimentary rocks deformed and metamorphosed at *c*. 1850 Ma during collision of the North Atlantic Craton with a lesser-known, likewise Archaean craton to the north (Kalsbeek *et al*. 1987; Taylor & Kalsbeek 1990; Kalsbeek & Nutman 1996; Connelly *et al*. 2000; van Gool *et al.* 2002a). The orogen extends from Søndre Strømfjord in the south, northward to Disko Bugt and possibly farther into the largely contemporaneous Rinkian fold belt (Fig. 1). The metamorphic grade associated with orogenesis decreases from granulite facies in the collisional core (the central Nagssugtoqidian orogen) to amphibolite facies in the southern foreland and the northern part of the orogen. Also the penetrative Palaeoproterozoic deformation diminishes toward the north in the northern Nagssugtoqidian orogen (NNO), and heterogeneous strain distribution may have been important in the preservation of pre-Nagssugtoqidian, i.e. Archaean structural fabrics and metamorphic assemblages and textures (van Gool *et al*. 2002a; Garde *et al*. 2004; Hollis *et al*. 2004; Piazolo *et al*. 2004; Mazur *et al*. 2006, this volume). As a consequence of the northward decrease in the Palaeoproterozoic thermal overprint and deformation, the NNO provides an opportunity for investigation of the pre-Nagssugtoqidian history of its Archaean components. In particular, its supracrustal belts can provide valuable information on the tectonic environment(s) of their formation, their relationship to the plate-tectonic configuration, and whether different parts of the craton experienced the same or different Archaean histories.

Here we investigate two supracrustal belts within the NNO – the kilometre-wide Ikamiut and Kangilinaaq belts – that crop out on the western and eastern sides of Sydostbugten in southern Disko Bugt (Fig. 1). Parts of the NNO were mapped by the Geological Survey of Greenland in the 1960s for its 1:500 000 scale geological map series (Noe-Nygaard & Ramberg 1961; Henderson 1969) and also by the Geological Survey of Denmark and Greenland (GEUS) in 2000–2003 for the 1:100 000 scale geological map series (see below). Henderson (1969) identified a complex map-scale fold structure that dominates the Ikamiut peninsula and adjacent inland areas in the western Sydostbugten region, and also outlined many of the dominant lithologies and large structural elements in the Kangilinaaq region.

In this paper we present geological, geochemical, geochronological and geophysical data from work carried out in the period 2000–2003 by GEUS mapping teams for the Kangersuneq and Ikamiut 1:100 000 scale geological map sheets (van Gool 2005; Garde in press); part of this work is reported in more detail in Keiding (2004). Aeromagnetic data for the Sydostbugten region are correlated with major lithological and structural elements. Geochemical data from amphibolites in the Kangilinaaq region interpreted as deformed and metamorphosed basaltic volcanic rocks, and interlayered pelitic rocks, are used to determine the likely depositional environment. Zircon Pb-Pb and U-Pb geochronology on granodioritic orthogneisses and a metasedimentary rock from the Ikamiut region is compared with existing data from the Ikamiut and Kangilinaaq regions. Finally, the implications for regional Neoarchaean tectonics are discussed.

Ikamiut belt and host rocks west of Sydostbugten

The Ikamiut belt is a deformed, kilometre-thick sequence of biotite schists, with less abundant siliceous and pelitic rocks, amphibolite and minor ultramafic rocks. The belt forms a ten kilometre-scale antiform in the north-western part of Sydostbugten (Fig. 2A). It is everywhere in contact with *c*. 2830–2760 Ma old, tonalitic to granodioritic orthogneiss (Pb-Pb whole rock, Kalsbeek *et al*. 1987; U-Pb zircon, Connelly & Mengel 2000 and this study), which dominates the region. The original nature of the contacts between the supracrustal belt and the regional orthogneiss is obscured by later ductile deformation (see also Østergaard *et al*. 2002). Rb-Sr data for 12 metasedimentary samples from this belt, near Ikamiut, gave an age of *c*. 1880 Ma for closure of the Rb-Sr system and a very high initial ^{87}Sr-^{86}Sr ratio of *c*. 0.712, suggesting that these rocks were deposited at around 2.8 Ga and isotopically strongly reset during Nagssugtoqidian metamorphism (Kalsbeek & Taylor 1999).

Structure

The structural pattern is dominated by kilometre-scale, closed, upright F_2 folds folding an S_1 foliation and associated with a moderate to intense, ENE-striking S_2 foliation (Fig. 2A). Preservation of S_1 fabrics is found in areas of low D_2 strain, typically within the cores of large F_2 folds. Outcrop-scale, parasitic F_2 folds associated with weak to moderately developed mineral lineations (L_2) plunge at shallow angles to the WSW. In the eastern Ikamiut region, L_2 lineations are shallow and, in some cases, plunge to the east. Some F_2 folds may be doubly plunging and/or refolded, consistent with localised outcrop-scale refolded

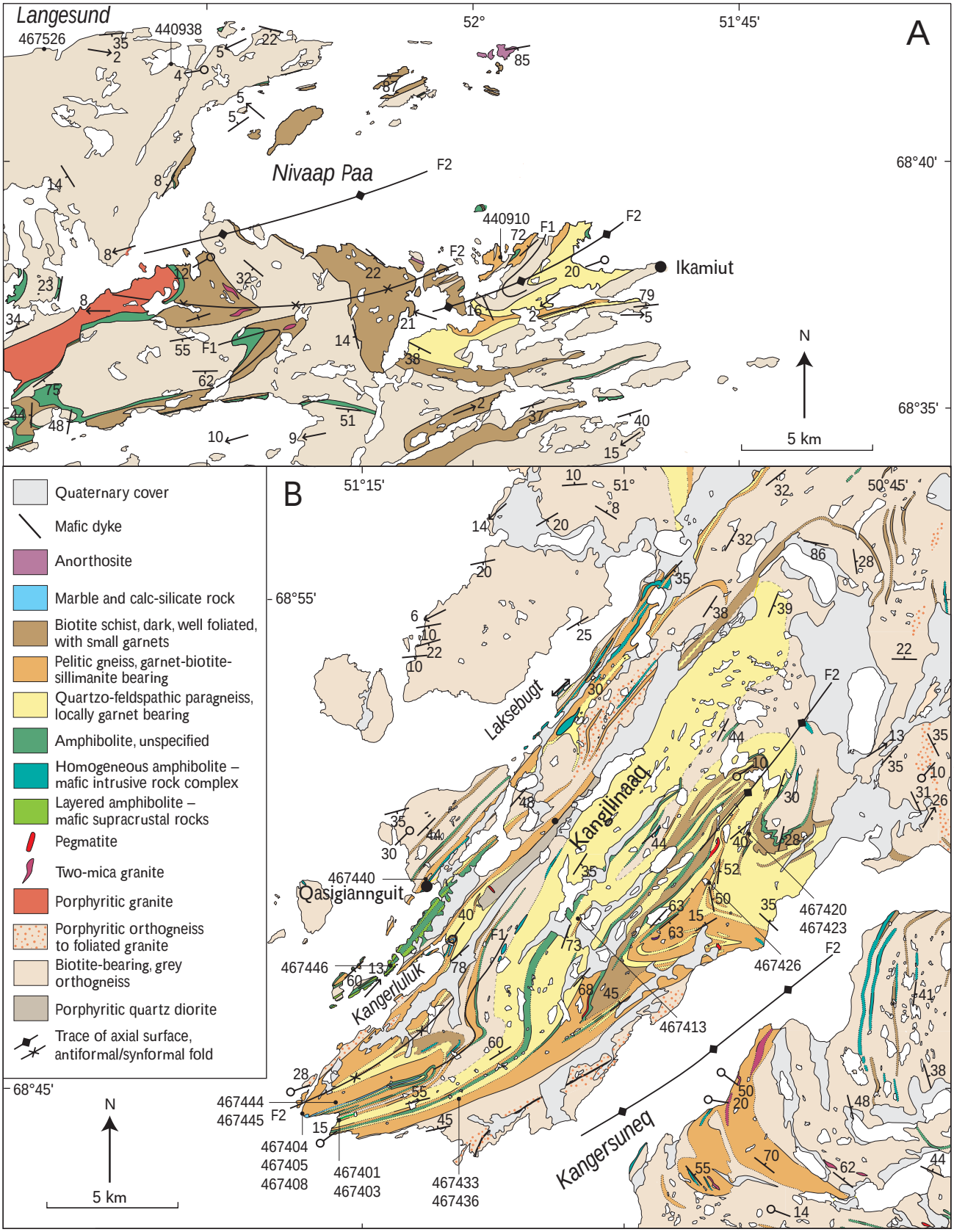

Fig. 2. Preliminary geological interpretation maps on (a) the Ikamiut region and (b) the Kangilinaaq peninsula, showing representative structural data, sample numbers and localities. For regional location see frames in Fig. 1.

folds. The kilometre-scale, upright F_2 folds are probably parasitic on the major antiformal structure that dominates the outcrop pattern. Ten to hundred metre-scale, shallowly W-plunging F_2 folds of flat-lying S_1 foliation are abundant in the tonalitic to granodioritic orthogneiss inland at the head of Nivaap Paa (Fig. 2A). These folds are difficult to trace for long distances along strike. The inland outcrop is relatively poor, and available outcrop suggests that some of the folds die out towards the west, apparently because of homogeneity and lack of ductility contrast within the orthogneiss.

Lithologies, mineral assemblages and fabrics

The tonalitic to granodioritic orthogneiss is a compositionally layered, medium-grained, pale pink and grey rock dominantly comprising plagioclase and quartz, with lesser K-feldspar and disseminated biotite. A medium- to coarse-grained gneissic layering (S_1) is discontinuous on a scale of metres to tens of metres and commonly displays intrafolial isoclinal folds. The orthogneiss typically also holds a moderate, ENE-striking S_2 foliation that is a partially to completely transposed S_1 fabric, and a weakly to moderately developed, shallow W-plunging L_2 mineral lineation. Medium- to coarse-grained, centimetre-scale granitic veins indicate variable D_2 strain: they form a layering that is typically transposed into S_2, but in some cases they are slightly discordant.

The supracrustal sequence is dominated by biotite schists to gneissic rocks that typically comprise plagioclase, quartz, biotite, and rarely garnet. Interlayered with these rocks occur local, more mica-rich and aluminous layers up to 20 m thick, which commonly display a schistose S_1 fabric. These rocks typically comprise biotite, plagioclase, quartz, muscovite, sillimanite, and garnet, with accessory tourmaline. Locally, in the most micaceous parts, a D_2 crenulation of S_1 biotite, plagioclase and quartz ± sillimanite is developed, with axial planes parallel to the dominant regional S_2 gneissosity of the tonalitic–granodioritic orthogneiss host, and fine-grained biotite and muscovite along the crenulations. Aggregates of fine-grained sillimanite and biotite in biotite-rich schists form blocky, centimetre-scale patches interpreted as pseudomorphs after andalusite. This suggests that the S_1 fabrics and assemblages were formed at low-pressure (< 3.85 kbar), lower amphibolite facies metamorphic conditions, followed by increasing temperature (and possibly also pressure) into sillimanite-grade conditions.

A distinct unit of siliceous paragneiss, locally garnet-bearing, is also volumetrically important. It is distinguished from the biotite schist/gneiss by its more quartz-rich and mica-poor composition. It is often difficult to distinguish this lithology from the tonalitic to granodioritic orthogneiss, particularly in inland areas where outcrop is poor.

Amphibolite layers, which are 10–50 m thick and laterally discontinuous on a kilometre-scale, are associated with the metasedimentary sequence. They commonly occur at or near boundaries between the metasedimentary rocks and orthogneiss. The amphibolites are medium grained and comprise hornblende with lesser plagioclase and quartz, and locally clinopyroxene ± garnet. In some cases they show distinct mafic–felsic layering, and they commonly contain thin (0.5–5 cm), discontinuous felsic layers.

A few isolated occurrences of intensely deformed anorthosite occur at tectonised boundaries between the tonalitic to granodioritic orthogneiss and metasedimentary rocks. The largest occurrence is in the northern island group of Nivaap Paa (Fig. 2A). The anorthositic rock is coarse grained and 'zebra-striped', and consists of hornblende and calcic plagioclase with a variably developed foliation and an intense linear fabric. The mafic parts are commonly boudinaged within the more felsic component.

An extensive body of medium- to coarse-grained granite is located within the hinge zone of the large antiformal structure along the southern coast of Nivaap Paa. The granite is porphyritic and white to red in colour, and holds a weak gneissose fabric. Its northern contact with the regional orthogneiss is tectonised and possibly tectonically repeated. The relatively undeformed nature of the granite suggests it intruded into the orthogneiss after formation of the regional gneissose fabric (S_2). The granite contains thin lenses and layers of medium-grained amphibolite, and is bounded to the south by a layer of amphibolite 50–400 m thick, the outcrop of which defines a tight synformal fold closure (Fig. 2A).

Kangilinaaq belt and host orthogneiss east of Sydostbugten

The Kangilinaaq peninsula (Fig. 2B) is dominated by a kilometre-scale synformal structure comprising a series of NE-trending, upright, isoclinal F_1 and F_2 folds that repeat a thick supracrustal sequence. The most common lithologies are quartzo-feldspathic and pelitic metasedimentary rocks, with lesser amphibolite and subordinate marble and calc-silicate rocks. An equivalent supracrustal sequence is found south of Kangersuneq fjord, on the southern limb of an antiformal fold running through the fjord. A lithologically distinct unit of amphibolite and associated metasedimentary rocks runs through the town

of Qasigiannguit in the west of the peninsula. For ease of reference this unit is named the Qasigiannguit amphibolite in the following. It is separated from the main supracrustal sequence by 200–500 m of high-strain Archaean orthogneiss. The significance of this high-strain zone in terms of the original supracrustal stratigraphy is uncertain, and thus the Qasigiannguit amphibolite may or may not be part of an originally continuous supracrustal series on the Kangilinaaq peninsula. For descriptive reasons the two supracrustal sequences are collectively termed the Kangilinaaq belt in the following.

Pelitic rocks from the main supracrustal sequence contain Archaean detrital zircon populations in the range 2820–2760 Ma, with a minimum depositional age constrained by an intrusive two-mica granite at 2723 ± 15 Ma (Thrane & Connelly 2006, this volume). Metamorphic zircon growth occurred at 1920–1820 Ma in various rocks (Keiding 2004; Thrane & Connelly 2006, this volume). Age data are addressed in more detail in the discussion.

Structure

The structural pattern is dominated by large, tight to isoclinal folds. Especially along the south-eastern side of the peninsula, the quartzo-feldspathic and pelitic rocks are intensely folded into upright folds on scales from decimetres to tens of metres with shallowly NE-plunging fold axes. Older, isoclinal, often intrafolial folds indicate that the upright folds are at least second-generation (F_2). A shear zone containing mylonitic orthogneiss bounds the supracrustal rocks to the south-east. It can be traced from the south-western part of the peninsula to half-way up Kangersuneq fjord, where it meets the water (Fig. 2B). Kinematic indicators and a lineation suggesting sinistral/top to the west movement are poorly developed in the shear zone. The continuation of the shear zone may be found in a poorly developed, but continuous SE-trending shear zone south of Kangersuneq fjord, marked by a sliver of metasedimentary rocks. North-west of the supracrustal sequence, no similar shear zone was found, although some smaller zones of high strain were recognised.

Lithologies, mineral assemblages and fabrics

The predominant regional lithologies are layered, grey tonalitic to granodioritic orthogneisses interleaved with supracrustal rocks. The orthogneisses contain variable proportions of plagioclase, quartz and biotite, with minor K-feldspar and hornblende. Compositional layering of orthogneiss with thin amphibolite layers interpreted as highly attenuated enclaves, give the rocks a layered appearance. The orthogneisses are intersected by concordant to slightly discordant, medium- to coarse-grained, centimetre- to half metre-scale granitic veins interpreted as derived from local melts. The orthogneisses show intrusive contacts into part of the supracrustal sequence (see below), although it is not certain that this relationship applies to all of the supracrustal rocks on the peninsula. The gneissic fabric of orthogneiss in the core of the peninsula is locally disturbed by pods and sweats of partial melt, which can contain millimetre-sized garnets. Garnet formation in the orthogneiss is restricted to the core of the peninsula, a region of abundant metasedimentary rocks. The garnet formation may be the product of contamination during partial melting of the metasedimentary rocks, either during intrusion of the precursors to the orthogneiss, or during metamorphism.

Variably deformed quartz diorite occurs in two localities. Typically it has tectonised contacts with the supracrustal rocks, but east of Qasigiannguit it has intrusive contacts to the latter and has yielded a U-Pb zircon emplacement age of 2801 ± 34 Ma (Thrane & Connelly 2006, this volume).

The main supracrustal sequence is dominated by medium-grained, quartzo-feldspathic metasedimentary rocks that commonly contain garnet. Where garnet is absent in these rocks, they are difficult to distinguish from the orthogneisses. The quartzo-feldspathic paragneiss alternates on metre- to 100 metre-scale with pelitic rocks, amphibolite and rare calc-silicate rocks. The pelitic rock comprises quartz, plagioclase, biotite, garnet, and sillimanite. Locally, it has a large component of granitic partial melt, commonly occurring in boudinaged lenses, indicative of upper amphibolite facies metamorphic conditions. Amphibolites are commonly dark and subtly layered, fine to medium grained and few metres to 50 m wide. Remnants of deformed pillows are locally present. In the eastern part of the sequence isolated lenses of metamorphosed ultramafic rocks occur in a few locations, commonly within amphibolites. They comprise predominantly amphibole and orthopyroxene, with or without clinopyroxene, olivine, phlogopite, and serpentinite. Minor calc-silicate rocks are layered, with variable grain size, and comprise calcite, phlogopite, quartz, tremolite and locally actinolite. Pelitic rocks in this sequence are commonly coarse grained and comprise quartz, biotite, garnet, plagioclase, and sillimanite. Large lumps of fibrous sillimanite (up to 3 cm in diameter) are likely pseudomorphs after andalusite. Rare pseudomorphs of sillimanite after kyanite were also found.

This may indicate variability in pressure conditions in the Kangilinaaq belt or prograde Barrovian-style metamorphism. Quartzo-feldspathic metasedimentary rocks in the central/northern part of the synform are coarse grained, heterogeneous, and rarely garnet-bearing.

The Qasigiannguit sequence comprises mafic and felsic metavolcanic rocks intercalated with clastic sequences and isolated layers and lenses of strongly deformed, zebra-striped anorthosite. The sequence is *c*. 700 m wide, trends SW–NE, and is well exposed on the islands south-west of Qasigiannguit. The rocks are isoclinally folded with an intrafolially folded gneissic fabric. As mentioned above it is separated from the predominantly clastic sequence of Kangilinaaq by 200–500 m of high-strain Archaean orthogneiss (Fig. 2B; see also below). In contrast with the main supracrustal belt, the metamorphic grade is lower amphibolite facies. The fine- to medium-grained, layered amphibolite contains hornblende and plagioclase, and minor clinopyroxene, epidote, biotite, quartz, and possibly also chlorite. Only along Laksebugt is the amphibolite locally garnet-bearing. Felsic layers can be up to several metres wide and contain predominantly plagioclase and quartz, with minor amphibole, white mica and titanite. Pelitic and semipelitic layers up to 50 m wide occur mainly on the islands south-west of Qasigiannguit. These layers are generally schistose and contain predominantly quartz, plagioclase, biotite and minor garnet, while sillimanite and muscovite are rare. In exposures 25 km north-east of Qasigiannguit, an outcrop of kyanite-bearing pelite shows no indications of replacement by sillimanite. This is the only known occurrence in the north-eastern part of the Nagssugtoqidian orogen of stable kyanite, although this mineral has also been described from Archaean supracrustal rocks within the southern part of the Rinkian fold belt (Garde & Steenfelt 1999). Fine-grained, dark grey biotite-rich schist/gneiss forms layers 50–80 m wide that grade locally into layered amphibolites. Homogeneous, medium-grained, greyish green, quartzo-feldspathic gneisses form layers up to 30 m wide that are generally platy and contain quartz, plagioclase, white mica, and amphibole. Their origin is uncertain. Their occurrence in a layered supracrustal sequence, without obvious intrusive contacts, could indicate that these rocks are also of supracrustal origin, but similar rocks in the main Kangilinaaq sequence grade into low-strain megacrystic granodiorite to quartz diorite. The contacts between the Qasigiannguit amphibolite and the regional Archaean orthogneiss are always tectonised, and their original contact relationships are uncertain. However, lenses of amphibolite, and locally also anorthosite, occur abundantly as inclusions in the regional Archaean orthogneiss close to its contacts with the supracrustal sequence. These lenses are unlikely to be tectonic because they occur in an irregular pattern, not along zones of high strain. It is more likely that they are xenoliths, suggesting that the orthogneiss precursors intruded into the supracrustal sequence.

Aeromagnetic characteristics

Aeromagnetic data covering the Ikamiut and Kangilinaaq regions (Thorning 1993) allow us to image geological features in terms of magnetic responses, also in areas covered by lakes, sea and overburden. A spacing of flight lines of 1 km and a survey altitude of 500 m control the resolution of the aeromagnetic data. In order to enhance the anomaly patterns from shallow-seated geological features, a separation filter has been applied (Jacobsen 1987). The filter enhances magnetic anomalies caused by geological features within a specific depth interval in the crust. The rationale of the filter is that the upward continuation of a potential field to a selected height represents the field from sources in the crust below half the selected height. The difference, or residual, between fields at two different heights can then be viewed as representing the field from sources within the corresponding depth interval in the crust. Thus, a total magnetic field that has been continued upward to a height of 2 km represents sources in the crust below 1 km. Likewise, the field observed at 500 m represents sources below 250 m. Consequently, the residual obtained from these two fields by subtraction represents an enhanced image of the anomaly pattern of geological features in the depth interval 250 m – 1 km. The resulting 'subsurface' total magnetic field for the Ikamiut–Kangilinaaq region is shown in Figs 3–5. In view of the fundamental ambiguity and complexity of the magnetic field separation, the filtering should only be used as a tool for detection of anomalies and discrimination of patterns, and qualitative interpretations should be supported by other types of geological data.

Aeromagnetic patterns in the Ikamiut region

The supracrustal rocks in the Ikamiut region appear as intermediate to low magnetic anomalies in the separation-filtered total magnetic field intensity map (–1 to –30 nT, A's in Fig. 4). The orthogneisses are expressed as slightly higher magnetic anomalies (5–20 nT, B and C in Fig. 4), although these show considerable variability that may be a consequence of differing contributions from other subsurface lithologies. From the aeromagnetic anomalies it is

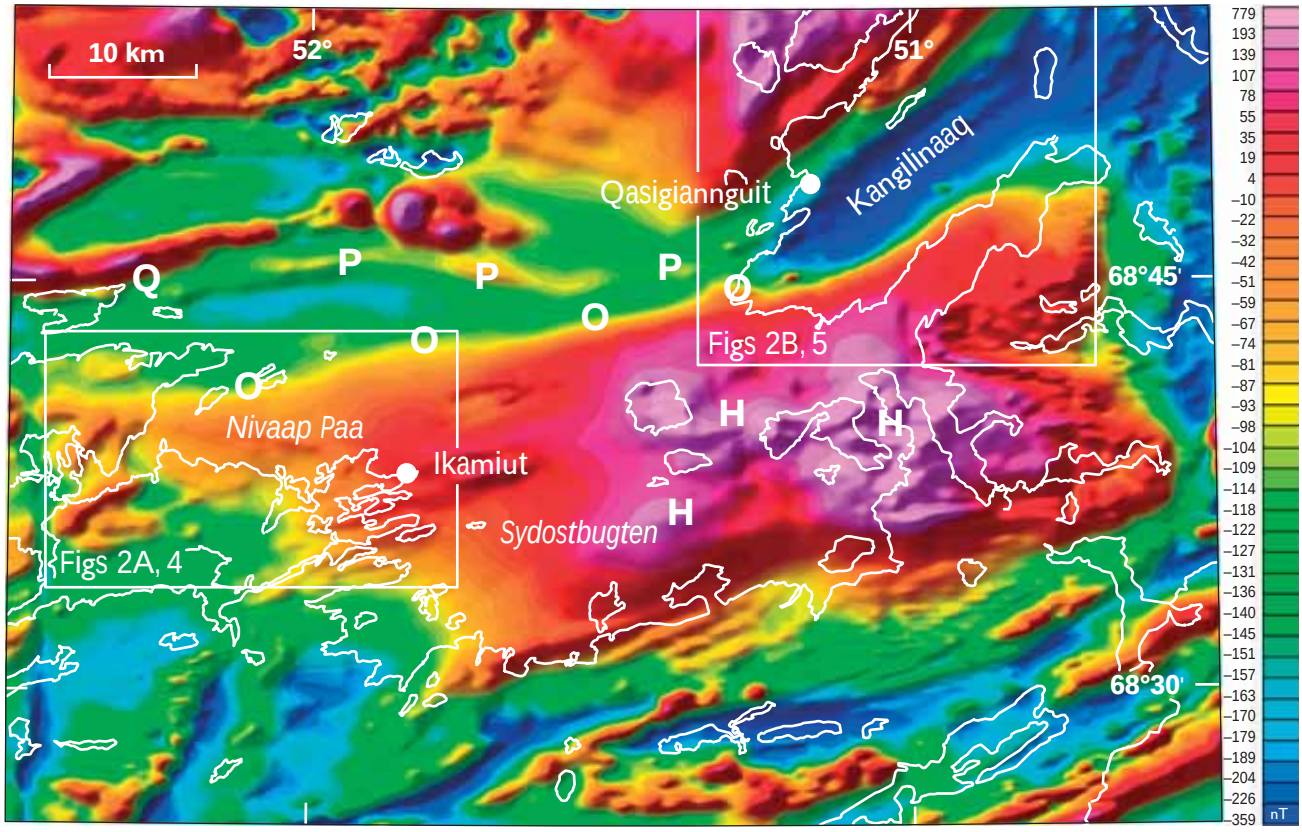

Fig. 3. Total magnetic field intensity for the Ikamiut and Kangilinaaq regions. The labels H, O, P and Q are referred to in the main text. A shadowing effect from NW (315°N) with an inclination of 45° has been applied. The areas of Figs 4 and 5 are outlined by white frames.

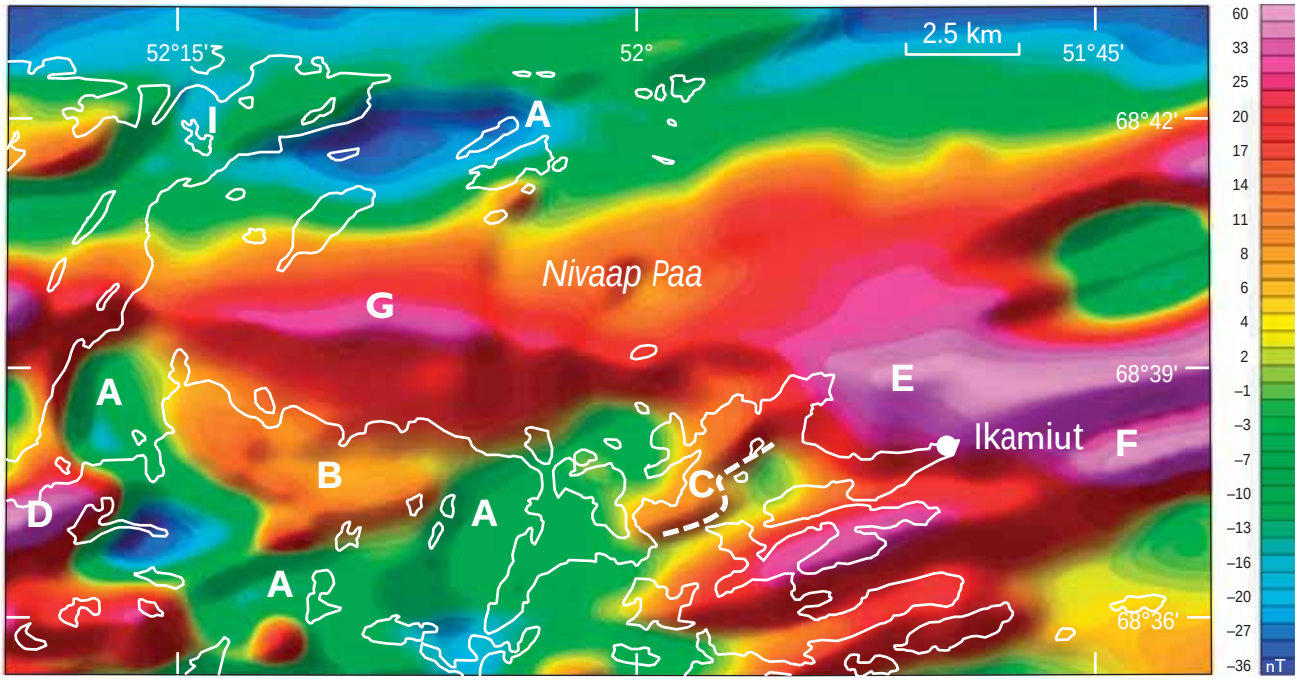

Fig. 4. The separation-filtered total magnetic field intensity in the interval from 0.250 m – 1 km for the Ikamiut area. Shadowing effect as in Fig. 3. The labels A–I are referred to in the main text.

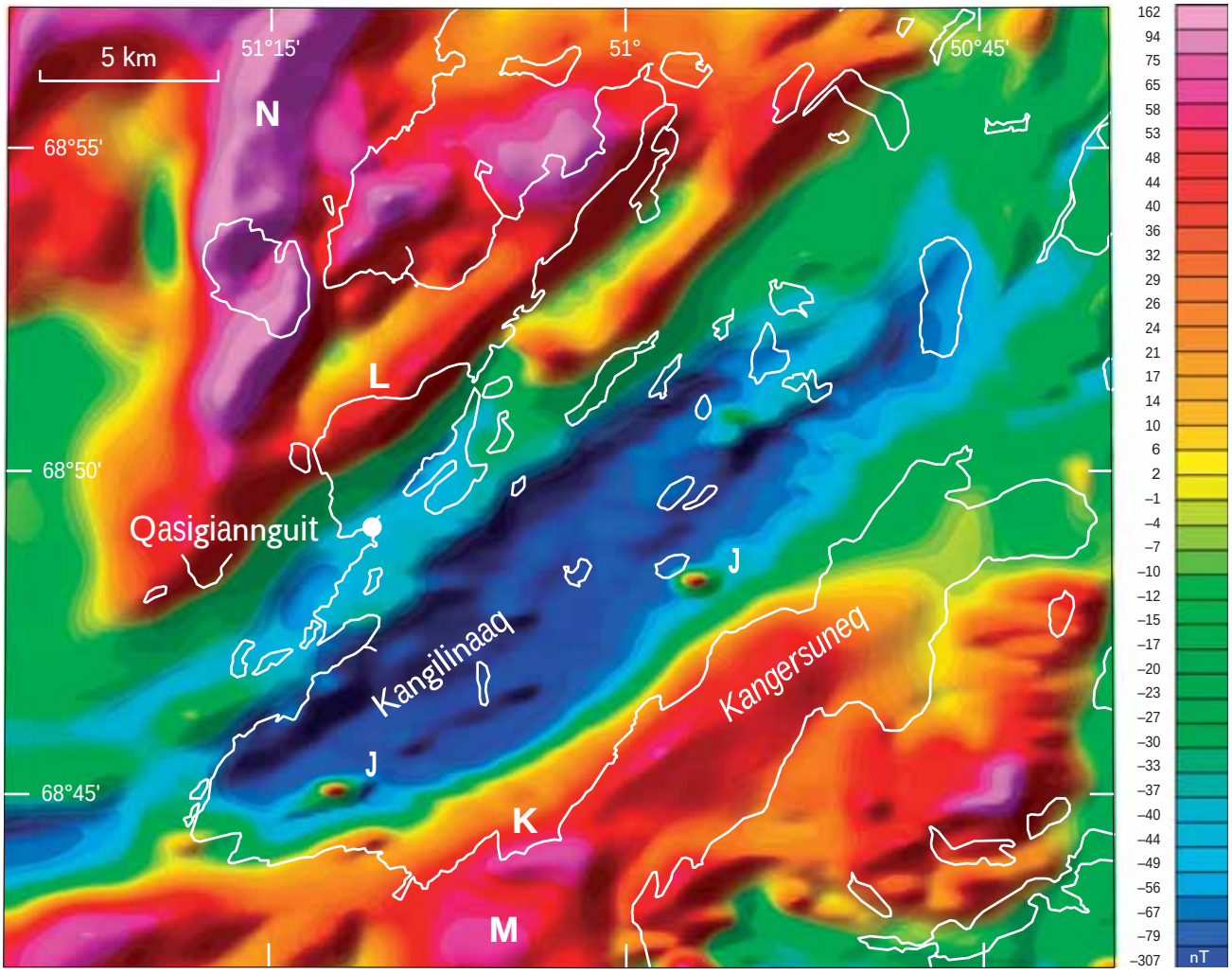

Fig. 5. The separation-filtered total magnetic field intensity in the interval from 0.250 m – 1 km for the Kangilinaaq area. Shadowing effect as in Fig. 3. The labels J–N are referred to in the main text.

possible to recognise folding of the orthogneiss (e.g. east of C, Fig. 4), which correlates closely with the geological mapping (Fig. 2A). Similarly, a strong magnetic low visible between B and D (Fig. 4) defines a refolded fold structure in pelitic gneiss identified during mapping. Exposed granitic rocks are visible as high positive anomalies (D, Fig. 4). Similar anomalies are visible beneath the sea north and east of Ikamiut and beneath the bay of Nivaap Paa (E, F and G, Fig. 4). The orthogneiss north of Nivaap Paa (I, Fig. 4) shows slightly lower magnetic anomalies than the orthogneisses to the south.

Aeromagnetic patterns in the Kangilinaaq region

The supracrustal belt on the Kangilinaaq peninsula appears as a distinct, rather homogeneous, low negative magnetic anomaly (–35 to –300 nT, Fig. 5), possibly reflecting the dominance of quartzo-feldspathic rocks with low magnetite contents. Small positive, short-wavelength, ovoid anomalies within the supracrustal rocks reflect small ultramafic bodies (J's, Fig. 5, too small to appear on the map of Fig. 2B). The biotite-bearing orthogneiss south of the supracrustal belt shows a positive magnetic anomaly (0–55 nT, K in Fig. 5). The change is rather abrupt and correlates with the ENE-trending mylonitic shear zone along the south-eastern margin of the supracrustal rocks close to the coast of the peninsula (see also Fig. 2B). The north-western boundary of the supracrustal belt on the opposite side of the peninsula, where supracrustal rocks and orthogneiss are interleaved, is less well defined. Farther north in the vicinity of Qasigiannguit, an abrupt change to a high positive magnetic anomaly field to the north-west corresponds with the northern contact of the amphibolite sequence against the orthogneiss (L in Fig.

5). The positive magnetic anomalies within the orthogneiss domains immediately north and south of the Kangilinaaq peninsula (M and N in Fig. 5) are much stronger than found within the orthogneiss in the north-eastern region of Fig. 5 (e.g. at 68°55′N, 50°45′W). Based on similar strong positive anomalies associated with granitic rocks in the Ikamiut area (Fig. 4) and the porphyritic granite on the south-western tip of the Kangilinaaq peninsula (Fig. 5), the former anomalies may correspond to large deep-seated granitic intrusives. Likewise, the large magnetic high at eastern Sydostbugten may represent granitic intrusive rocks hidden 1–2 km below the present surface (H's, Fig. 3; Thorning 1993; Nielsen & Rasmussen 2004).

Geochronology

Zircon separates from three samples from the Ikamiut region were analysed to determine (1) the age of emplacement of the regional tonalitic to granodioritic orthogneiss, (2) the age distribution, provenance and minimum age of deposition of the sedimentary precursor to the Ikamiut metasedimentary rocks, and (3) the timing of metamorphism. Samples of two granodioritic orthogneisses and a quartzo-feldspathic metasedimentary rock were analysed, see below. Sample descriptions of these and other rocks are given in Table 1, and the age data are presented in Tables 2–3 and Figs 6–7. All age data in the text are quoted with 2σ absolute uncertainty.

Methodology

Samples were crushed and sieved to < 400 µm. The fraction < 45 µm was removed via washing and sieving and the remaining sample panned in water to concentrate the heavy fraction. The heavy, nonmagnetic fraction was separated using heavy liquids (3.30 gcm^{-3}) and a Frantz magnetic separator. Zircons were hand-picked and mounted in epoxy resin. For secondary ion mass spectrometry (SIMS) analysis, grains were mounted together with 1065 Ma zircons from reference sample 91500, Ontario, Canada (Wiedenbeck *et al*. 1995). For laser inductively-coupled plasma mass spectrometry (LA-ICP-MS) analysis no zircon standard was used. The mounted samples were ground to expose the mid-sections of the zircons and polished. The polished samples were examined using backscattered electron (BSE) imaging on a Philips XL 40 scanning electron microscope at GEUS, operating at 20kV and a working distance of 10 mm. Backscattered electron

Table 1. Sample descriptions

Sample	Region	Rock type	Paragenesis
		Amphibolite	
467403	Kangilinaaq	Fine-grained, layered amphibolite	hbl-pl ± cpx ± grt, accessory Fe-Ti oxides
467405	Kangilinaaq	Fine-grained, layered amphibolite	
467413	Kangilinaaq	Fine-grained, layered amphibolite	
467426	Kangilinaaq	Fine-grained, layered amphibolite	
467436	Kangilinaaq	Fine-grained, layered amphibolite	
467440	Kangilinaaq	Fine-grained, layered amphibolite	
467444	Kangilinaaq	Fine-grained, layered amphibolite	
467445	Kangilinaaq	Fine-grained, layered amphibolite	
467446	Kangilinaaq	Fine-grained, layered amphibolite	
		Orthogneiss	
440938	Ikamiut	Medium-grained granodioritic orthogneiss	pl-qtz-ksp-bi
467526	Ikamiut	Medium-grained granodioritic orthogneiss	pl-qtz-ksp-bi
467401	Kangilinaaq	Medium-grained tonalitic orthogneiss	pl-qtz-bi
		Metasedimentary rocks	
440910	Ikamiut	Quartzo-feldspathic gneiss	pl-qtz-grt-bi, minor sill-ksp
440931	Ikamiut	Quartzo-feldspathic gneiss	pl-qtz-bi, minor ksp-mag. Bi partly replaced by chl
467503	Ikamiut	Quartzo-feldspathic gneiss	pl-qtz-bi, minor ksp-mag-mu
467404	Kangilinaaq	Garnet-bearing schist	qtz-pl-bi-sill-grt. Bi partly replaced by sill
467408	Kangilinaaq	Cummingtonite gneiss	qtz-pl-bi-cu, minor hbl
467417	Kangilinaaq	Biotite-hornblende gneiss	qtz-pl-bi-hbl
467420	Kangilinaaq	Fine-grained schist	qtz-pl-bi-ep, accessory al & zn
467423	Kangilinaaq	Hornblende gneiss	hbl-pl, minor qtz, bi
467433	Kangilinaaq	Hornblende gneiss	hbl-pl, minor qtz, bi

Mineral abbreviations: al: allanite, bi: biotite, cpx: clinopyroxene, cu: cummingtonite, ep: epidote, grt: garnet, hbl: hornblende, ksp: K-feldspar, mag: magnetite, mu: muscovite, pl: plagioclase, qtz: quartz, sill: sillimanite, ti: titanite, zn: zircon.

Table 2. Zircon LA-ICP-MS ^{207}Pb-^{206}Pb data

Spot	^{206}Pb (cps)	$^{207}Pb/^{206}Pb$	Age (Ma)	2σ %
440938 Granodioritic orthogneiss				
1	44913	0.207628	2847	4.8
2	54464	0.206401	2843	6.1
3	51744	0.211202	2865	10.9
5	66847	0.205833	2818	12.1
6	45663	0.239096	3072	7.3
7	114515	0.203027	2811	4.9
10	29662	0.206933	2835	8.2
12	81235	0.200267	2785	5.6
15	63304	0.204663	2825	8.7
16	58962	0.203500	2813	7.4
17	32961	0.211432	2888	7.4
20	86073	0.205326	2830	9.7
21	125993	0.199600	2796	4.5
25	60136	0.185466	2664	6.1
26	48587	0.207014	2855	5.6
27	98098	0.202412	2838	8.0
28	46100	0.198084	2836	11.7
29	44476	0.209520	2878	6.4
30	55984	0.205825	2836	9.9
31	52515	0.204633	2835	7.3
33	60481	0.205708	2838	7.2
34	41693	0.217275	2967	29.6
40	16473	0.210866	2905	33.5
41	63641	0.205836	2847	6.9
42	26576	0.199429	2802	10.4
43	34970	0.210589	2882	6.9
44	66299	0.200725	2807	4.9
47	76450	0.185001	2778	5.5
48	344404	0.196981	2819	6.9
50	94026	0.206532	2859	4.6
54	32535	0.206805	2838	17.7
55	18887	0.185070	2753	19.3
57	45001	0.201119	2811	5.3
59	63523	0.203583	2830	8.1
60	35435	0.205041	2842	6.2
61	23531	0.190093	2715	6.2
63	112296	0.208790	2878	4.6
64	39902	0.195071	2763	6.6
74	19592	0.202403	2820	6.2
75	30652	0.204612	2837	11.0
77	41961	0.195999	2774	6.8
78	64028	0.206406	2860	6.1
80	30243	0.209704	2877	6.2
81	106313	0.203552	2844	6.4
82	47863	0.206121	2857	7.4
83	58886	0.201354	2817	6.6
84	119357	0.209519	2882	4.0
86	93017	0.206130	2857	4.8
87	59542	0.208843	2878	4.8
88	80384	0.190889	2738	6.0
89	56425	0.198658	2797	6.6
90	52868	0.194667	2773	5.8
91	54794	0.203058	2825	6.2
92	86828	0.211233	2895	4.7
93	86433	0.207258	2863	4.4
94	41347	0.203007	2830	5.5
467526 Granodioritic orthogneiss				
5	56698	0.200720	2804	5.3
6	33787	0.193076	2748	6.6
7	55326	0.195289	2762	4.8
8	76699	0.182851	2652	4.9
10	31196	0.183045	2654	6.6
11	4904	0.204104	2807	12.9
13	39648	0.191787	2718	5.5
15	40707	0.202256	2816	5.0
17	29635	0.217163	2844	19.1
18	6853	0.206028	2827	14.9
19	9339	0.206467	2995	5.7
440910 Metasedimentary rock				
1	35535	0.200401	2828	6.5
2	31197	0.211066	2824	10.1
3	41461	0.193703	2741	6.1
4	30241	0.204419	2821	6.0
5	25534	0.191383	2718	5.6
6	46366	0.198531	2774	6.1
7	86549	0.207000	2846	5.7
8	48635	0.201767	2807	5.3
9	36751	0.209132	2858	7.0
10	27744	0.183921	2654	9.9
11	43029	0.194263	2742	6.7
12	29314	0.172110	2520	8.6
13	47160	0.206249	2841	5.9
14	49306	0.201659	2804	7.0
15	29978	0.198089	2779	6.0
17	53134	0.194413	2748	5.4
18	27856	0.201215	2810	6.9
19	30082	0.205162	2842	5.9
20	55684	0.198413	2780	5.1
21	147594	0.191303	2722	5.3
22	25436	0.210142	2870	7.0
23	29257	0.196016	2766	7.0
24	20655	0.203877	2826	6.4
25	26159	0.201727	2796	6.6
26	82319	0.215426	2917	4.5
27	112103	0.194672	2751	5.1
30	15491	0.200465	2794	7.1
31	21709	0.204749	2831	8.0
32	14364	0.206770	2843	11.0
33	41967	0.201274	2800	6.8
34	56320	0.189864	2710	5.6
35	23757	0.202176	2801	9.1
36	30037	0.201451	2808	6.6
37	31254	0.193787	2730	7.6
38	22041	0.205579	2827	10.1
39	52491	0.162084	2504	10.1
40	40780	0.194811	2741	5.7
42	61409	0.195555	2747	4.9
43	103057	0.171459	2534	10.0
44	40828	0.200096	2744	7.8
45	58477	0.197715	2764	5.3
46	20270	0.206049	2843	8.7
47	33049	0.196133	2748	6.5
48	28126	0.193760	2738	6.3
50	19721	0.207732	2845	6.6
51	86891	0.232092	2997	11.6
52	58228	0.201806	2799	5.0
53	50522	0.190800	2710	5.8
54	60856	0.195334	2736	5.6
55	35515	0.198275	2772	5.4
56	51577	0.196653	2758	5.9
58	27007	0.203361	2811	5.7
59	49414	0.202192	2798	5.8
62	10375	0.207836	2855	9.5
63	120563	0.189864	2717	4.2
64	23252	0.187771	2722	7.0
65	26567	0.202492	2801	6.5
69	89976	0.191213	2728	4.7
70	25130	0.199809	2796	6.1
71	68881	0.206577	2861	4.6
72	53407	0.199076	2805	5.1
73	51707	0.194570	2755	4.9
74	67393	0.179579	2625	5.3
75	30132	0.198104	2773	6.6
76	36875	0.197163	2802	7.8
77	28362	0.198893	2790	5.4
78	27133	0.201214	2812	5.7
79	133087	0.188329	2702	4.7
80	45162	0.206677	2856	4.4
81	51961	0.194173	2749	4.6
83	27444	0.201457	2807	5.6
84	26057	0.208900	2868	5.4
85	31842	0.198490	2789	7.0
86	114220	0.180764	2635	5.5
87	62748	0.189371	2717	5.5
88	42113	0.198204	2782	5.2
89	24400	0.199600	2793	6.6
90	29322	0.208314	2861	5.3
91	75430	0.205029	2835	6.0
93	24848	0.198066	2773	6.3
95	60703	0.191617	2717	6.7
96	40762	0.207364	2850	4.1
97	131809	0.193200	2737	6.3
98	43657	0.197222	2778	5.6
99	17404	0.199360	2767	19.2

Table 3. Zircon ion probe (SIMS) U-Th-Pb data

Spot	U ppm	Th ppm	Pb ppm	Th/U measured	f^{206} %	$^{207}Pb/^{206}Pb$	σ %	$^{207}Pb/^{235}U$	σ %	$^{206}Pb/^{238}U$	σ %	Discordance % (conventional)	Ages (Ma) $^{207}Pb/^{206}Pb$	Ages (Ma) σ
440938 Granodioritic orthogneiss														
3	155	94	113	0.607	0.04	0.19819	0.28	14.5789	1.06	0.53352	1.03	–2.4	2811.3	4.6
4	575	274	417	0.502	0.07	0.19781	0.18	14.8262	1.04	0.54361	1.03	–0.4	2808.2	2.9
8	192	24	127	0.117	0.05	0.19575	0.28	14.5329	1.07	0.53845	1.03	–0.6	2791.1	4.6
14	164	23	109	0.140	0.02	0.19767	0.38	14.7352	1.09	0.54065	1.03	–0.9	2807.1	6.1
20a	206	56	134	0.222	0.09	0.19216	0.30	13.6935	1.07	0.51684	1.03	–3.3	2760.7	5.0
24	175	37	117	0.170	0.05	0.19891	0.31	14.7222	1.07	0.53682	1.03	–2.1	2817.2	5.0
29	578	153	384	0.217	0.23	0.19498	0.17	14.2171	1.04	0.52885	1.03	–2.1	2784.6	2.8
41	632	35	391	0.054	0.01	0.19138	0.14	13.5355	1.04	0.51295	1.03	–3.8	2754.1	2.4
54	273	155	199	0.555	0.09	0.19767	0.29	14.6540	1.07	0.53768	1.03	–1.5	2807.0	4.8
66	251	227	191	0.878	0.07	0.19836	0.23	14.3381	1.05	0.52425	1.03	–4.2	2812.7	3.7
72	203	158	150	0.762	0.09	0.19789	0.29	14.2560	1.07	0.52248	1.03	–4.3	2808.9	4.7
76	157	49	107	0.307	0.02	0.20014	0.33	14.6609	1.09	0.53127	1.04	–3.5	2827.4	5.4
440910 Metasedimentary rock														
22	850	51	526	0.057	0.01	0.18523	0.20	13.1609	1.78	0.51532	1.77	–0.9	2700.3	3.4
29	480	2	308	0.002	0.03	0.18986	0.27	14.0987	1.79	0.53857	1.77	1.6	2740.9	4.4
42	609	3	390	0.003	0.05	0.18800	0.22	13.9521	1.78	0.53823	1.77	2.3	2724.8	3.6
54	554	2	344	0.004	0.01	0.18507	0.22	13.3561	1.78	0.52342	1.77	0.7	2698.8	3.6
58c	106	32	71	0.275	0.23	0.19043	0.43	14.0439	1.82	0.53488	1.77	0.7	2745.9	7.1
58r	610	2	378	0.003	0.04	0.18916	0.21	13.6001	1.79	0.52146	1.77	–1.3	2734.8	3.5
82	1178	7	730	0.004	0.07	0.18473	0.17	13.3129	1.78	0.52267	1.77	0.7	2695.8	2.9

Errors on ratios and ages are quoted at the 1σ level.
c: core; r: rim; f^{206} %: The fraction of common ^{206}Pb, estimated from the measured ^{204}Pb.
Discordance %: Degree of discordance of the zircon analysis (at the centre of the error ellipse).

(BSE) images of some of the analysed grains showing sites of analysis and ages obtained are presented in Fig. 6.

All three samples were analysed at GEUS using a PerkinElmer 6100 DRC quadrupole inductively-coupled plasma mass spectrometer combined with a Cetac LSX 200 laser ablation unit based on a solid-state Nd-YAG laser, emitting at a wavelength of 266 nm. The laser was operated at 20 Hz with a spot size of 30 µm, producing pits of *c*. 50 µm depth. The masses ^{208}Pb, ^{207}Pb, ^{206}Pb, and ^{204}Pb were analysed in line scans run at 1 µm per second. Each analysis comprised 150 time-resolved replicates (duration of total analysis 150 s). In the case of small grains with diameters < 100 µm, only 100 replicates over 100 s were collected. If inconsistencies in the measured ratios were identified within the time span of each analysis, such as spikes relating to inclusions, or significant changes in Pb-Pb ratios indicative of sampling of different age zones, then the whole analysis was discarded. The analyses were standardised against NIST 610 glass (Pearce *et al*. 1997) to account for instrument drift. The influence of common Pb cannot be assessed using this method, since ^{204}Pb was generally below the detection limit. Also, because U isotopes could not be measured, the significance of Pb loss cannot be assessed, and therefore the ages determined should be regarded as minimum ages. In addition, the age resolution on any individual analysis was restricted owing to relatively low count rates obtained. However, it is a great advantage of the LA-ICP-MS method that a large number of analyses can be made within a short time period, allowing analysis of large numbers of grains in samples with isotopically simple zircon. The LA-ICP-MS age data are presented in Table 2 and as histograms coupled with relative probability curves (Fig. 7).

SIMS analysis of zircon from two samples (440938, 440910) was carried out using a CAMECA IMS 1270 secondary ion mass spectrometer at the NORDSIM laboratory, Swedish Museum of Natural History, Stockholm. The polished zircon mounts were coated with a *c*. 30 nm layer of gold. Analytical procedures and common lead corrections are similar to those described by Whitehouse *et al*. (1997). A primary O^{2-} ion beam is focussed into a spot with a diameter of 20 µm that sputters material from the sample to leave a flat-bottomed crater. Positive ions sputtered from the crater are extracted and mass-separated into the peaks of interest: $^{90}Zr_2{}^{16}O$, ^{204}Pb, ^{206}Pb, ^{207}Pb, ^{208}Pb, ^{238}U, $^{232}Th^{16}O$, and $^{238}U^{16}O$. Calibrations of Pb/U ratios are based on the observed relationship between Pb/U and UO_2/U. Weighted average $^{207}Pb/^{206}Pb$ ages were calculated using ISOPLOT (Ludwig 2000). SIMS age data are presented in Table 3 and on Tera-Wasserburg diagrams in Fig. 7.

Orthogneiss

The two samples of granodioritic orthogneiss selected for geochronology (440938 and 467526) were collected at the south coast of Langesund (Fig. 2A). Sample descriptions and chemical composition are presented in Tables 1 and 4. Sample 440938 yielded abundant zircon and contains common thin, transposed granitic layers, whereas sample 467526 does not contain such granitic leucosome. The zircons from both samples are 100–600 µm (mostly *c*. 200–300 µm) in length and translucent with a heterogeneous orange colour. The crystals are euhedral with slightly rounded terminations and aspect ratios from 1:2.5–1:4, typically *c*. 1:3. Broad oscillatory zones *c*. 10–30 µm wide are very common, with rare development of bright, presumably metamorphic rims (see below). The zircons are commonly weakly to moderately fractured, both concentrically and radially, and often show partial fracture healing within bright oscillatory zones (Fig. 6).

LA-ICP-MS analyses of 57 oscillatory zoned grains from sample 440938 give a weighted mean age of 2831 ± 23 Ma (2σ, MSWD = 0.36; Table 2; Fig. 7A). Ten SIMS analyses of cores of oscillatory zoned grains and two of bright rims reveal more age complexity, with seven of the cores yielding an important 2820–2810 Ma age component (Table 3; Fig. 7B, black data ellipses). Four of these seven analyses lie slightly off concordia. Another, slightly older and likewise discordant grain (2827 Ma, blue in Fig. 7B) belongs to the 2831 ± 23 Ma LA-ICP-MS age group. Many of the analysed grains show slight discordance indicating partial Pb loss, the timing of which is unclear from the data available. Two bright rims with significantly younger ages of 2761 ± 10 Ma and 2754 ± 5 Ma are interpreted as metamorphic. This is supported by the very low Th/U of the latter (0.054), though the former is not anomalous in this respect (Th/U = 0.22). The SIMS data are slightly but significantly younger than the LA-ICP-MS data for the same sample (but from different analysed grains), although the 2σ error on the LA-ICP-MS age spectrum encompasses most of the SIMS data. It is difficult to establish the reason for this, particularly given the apparent complexity of the zircons (Fig. 7B). It is possible that a larger proportion of older material has been sampled in the LA-ICP-MS work. It may also be that matrix effects had some influence in standardising zircon data against NIST610 glass, though such effects are not generally regarded as significant.

The few zircons separated from sample 467526 were analysed via LA-ICP-MS. Eleven analyses of cores displaying oscillatory zonation yield a poorly constrained weighted mean age of 2741 ± 53 Ma (2σ, MSWD = 0.55; Fig. 7C).

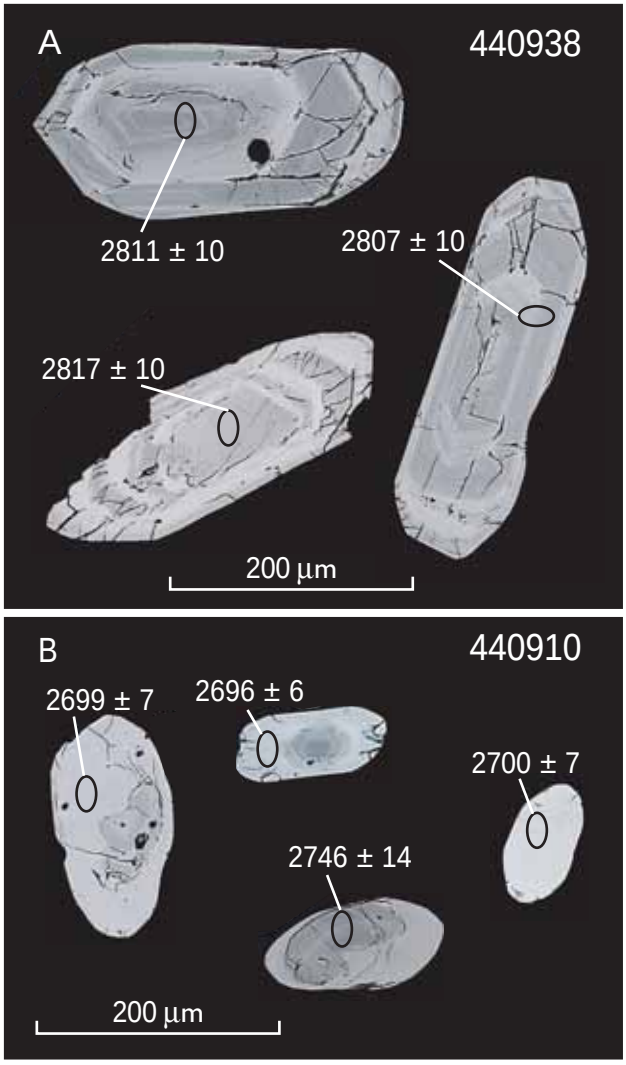

Fig. 6. Backscattered electron images of zircons in samples 440938 (orthogneiss) and 440910 (metasediment) analysed via SIMS, showing analysed areas and ages obtained.

It might be considered that the large analytical error for this sample leaves room for age complexity, possibly involving analysis of both inherited grains and Pb loss (similar to sample 440938). However, all analyses statistically belong to the same population, and there are no significant differences in internal zircon morphology that might account for different age groups.

Metasedimentary rocks

Sample 440910 from the Ikamiut belt (Fig. 2A) is a medium-grained, garnet-bearing quartzo-feldspathic, gneissic rock. Colourless, pale yellow and pale pink zircon grains are abundant. They are elongate and generally 100–200

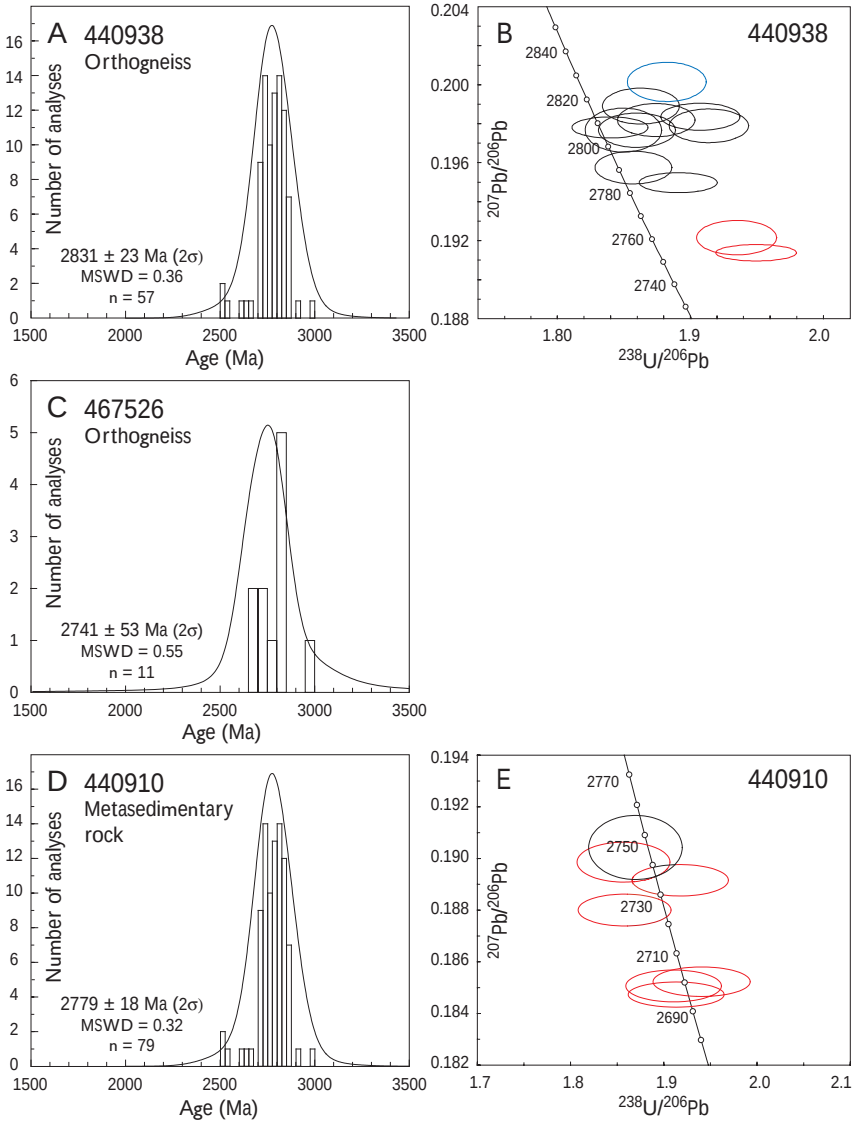

Fig. 7. LA-ICP-MS $^{207}Pb/^{206}Pb$ histograms and SIMS U-Pb Tera-Wasserburg concordia plots of zircon age data from the Ikamiut region. A: Histogram of $^{207}Pb/^{206}Pb$ ages from orthogneiss sample 440938. B: Tera-Wasserburg plot for orthogneiss sample 440938 showing nine cores of oscillatory-zoned grains (black), an older core (blue), and two bright rims (red). C, D: Histograms of $^{207}Pb/^{206}Pb$ ages from orthogneiss 467526 and metasedimentary sample 440910. E: Tera-Wasserburg plot for metasedimentary sample 440910 showing one core (black) and six metamorphic rims (red). The histogram bin size is 25 Ma (A, D) or 50 Ma (C). Error ellipses on concordia diagrams are drawn at 68.3% confidence (1σ).

µm in length, with rounded terminations and aspect ratios of 1:1–1:3, typically *c.* 1:2. BSE imaging reveals relatively wide (*c.* 10–30 µm) oscillatory zoned cores with moderate to well-developed bright rims *c.* 10–60 µm wide, which in many cases have annealed former fractures (Fig. 6).

^{207}Pb-^{206}Pb ages from 87 LA-ICP-MS analyses of oscillatory zoned zircon cores are shown in Fig. 7D. The vast majority (79) define a tightly clustered peak at *c.* 2800 Ma. The complete age range spans 2997–2520 Ma. The youngest ages (< 2700 Ma) may reflect mixed core–rim data, although most of them are statistically within the main age population. If a few anomalous old and young ages are disregarded, a weighted mean age of 2779 ± 18 Ma is obtained (2σ, MSWD = 0.32, n = 79). This group is interpreted as comprising a homogeneous population of detrital zircons, consistent with local derivation from orthogneiss of this age (see above). Seven SIMS analyses, of one core with oscillatory zonation and six bright rims, all fall on concordia (Fig. 7E). The core gives the oldest age of 2746 ± 14 Ma (Th/U = 0.275). The six analyses of bright rims give ages between 2741 ± 9 and 2696 ± 6 Ma. All have very low Th/U (0.004–0.06), consistent with a metamorphic origin. These metamorphic ages are comparable to the few young ages also identified in the LA-ICP-MS analyses, and suggest that this sample underwent metamorphism at *c.* 2740–2700 Ma, shortly after its deposition. An alternative, and in our view less likely interpretation is that the metamorphic rims were developed during metamorphism of the source rock prior to erosion and deposition of the sediment.

Geochemistry

Whole-rock geochemical analysis of amphibolites, felsic orthogneiss and metasedimentary rocks from the Ikamiut and Kangilinaaq regions was undertaken to (a) geochemically characterise these rock types, (b) investigate the likely tectonic environment of formation and provenance of the amphibolites and metasedimentary rocks, and (c) investigate likely regional correlations. Sample descriptions are presented in Table 1, and major and trace element compositions in Table 4.

Analytical procedure

Major and trace element analyses (Table 4) were performed by GEUS. The samples were ground in tungsten (Ikamiut samples) or agate (Kangilinaaq samples) mills, and dried. For major elements the rock powders were fluxed with sodium tetraborate and fused to glass discs and analysed with a Philips PW1606 X-ray fluorescence (XRF) mass spectrometer. Na and Cu were determined by atomic absorption spectrometry, and volatiles were analysed by gravimetry. Refer to Kystol & Larsen (1999) for the complete analytical procedure. For trace element analyses, powdered samples were brought into solution and analysed using a PerkinElmer 6100 DRC Quadrupole ICP-MS instrument. For the Ikamiut samples Zr, Cr, REEs and Hf were determined by dissolving a piece of the borate glass used in the major element XRF analyses, in order to obtain complete contributions of these elements from chromite and zircon. The ICP-MS results were corrected for the relevant oxide interferences using BHVO-1 and GH as standards.

For the Kangilinaaq samples some trace elements were also analysed by XRF performed directly on pressed powder tablets at the Geological Institute, University of Copenhagen, using a Phillips PW 1400 XRF spectrometer. The data were corrected for matrix variations using the major element compositions, and AGV-1 was run as standard.

Orthogneisses

Two orthogneiss samples from the Ikamiut region were analysed (440938 and 467526), and one from Kangilinaaq (467401; Table 4a; Fig. 2). The two Ikamiut samples show very similar granodioritic major element chemistry, while the Kangilinaaq sample is more tonalitic. The Kangilinaaq sample has low REE concentrations and a fairly steep REE curve with La_N/Lu_N ~ 16 (Fig. 8B). In contrast, the two Ikamiut samples have higher REE concentrations and significant negative Eu anomalies, consistent with the more evolved composition of these rocks.

Amphibolites from the Kangilinaaq belt

Nine amphibolites *s.s.* from the Kangilinaaq belt were analysed for major and trace elements (Table 4a); no amphibolite samples have been analysed from the Ikamiut region, where amphibolites only constitute a minor component of the supracrustal rocks. The nine samples from Kangilinaaq show only a small range in chemical composition. They have relatively primitive signatures with low SiO_2 (46–49 wt%) and high MgO (7–11 wt%), and flat REE patterns that group tightly around ten times chondrite values (Fig. 8A). Their Ti/V ratios display a narrow range of 16–19, and in a Ti-V diagram (Shervais 1982) they plot just within the island arc field (Fig. 9). The positive correlation between Ti and V could reflect fractionation of olivine and plagioclase. The geochemical resemblance between all nine samples and their well-defined Ti/V trend are consistent with formation within a single volcanic suite.

Metasedimentary rocks and hornblende-bearing gneisses from the Kangilinaaq belt

Metasedimentary sample 467404 is characterised by high alumina (19 wt%) coupled to low CaO (0.7 wt%) and high concentrations of REE and Ba (605 ppm), consistent with a clay-rich precursor. The REE curve is steep (La_N/Lu_N = 30, La = 140 times chondrite), and has a significantly negative Eu anomaly. Sample 467420 is siliceous (75 wt% SiO_2), consistent with a relatively mature sedimentary precursor. Its REE concentrations lie just below those of sample 467404, with a similar steep REE pattern. For sample 467417, both major and trace elements agree well with the average composition of Archaean mudstone from Taylor & McLennan (1985, table 7.8). The REE curve resembles that of sample 467408 (see below), although it has slightly lower concentrations of the HREE.

The hornblende-bearing gneisses 467423 and 467433 were collected from thin (< 1 m) amphibolite units within metasedimentary sequences. The geochemical compositions of these two samples are close to those of the nine amphibolite samples described above, and they can only be distinguished from the latter by their higher concentrations of LREE, Ba, and Sr, and higher K_2O and Rb in

Table 4a. Chemical analyses of amphibolite and orthogneiss

	Amphibolite, Kangilinaaq belt									Orthogneiss		
	467403	467405	467413	467426	467436	467440	467444	467445	467446	440938	467526	467401
SiO_2	48.73	48.72	49.3	46.86	48.39	47.37	48.01	48.25	46.00	71.93	71.70	68.86
TiO_2	1.03	0.87	0.83	0.60	0.64	0.66	0.90	0.88	0.75	0.24	0.39	0.22
Al_2O_3	13.16	15.81	14.61	16.21	15.68	16.36	13.29	12.18	16.25	14.58	14.64	16.93
Fe_2O_3	1.67	2.54	2.7	1.88	2.13	2.79	1.90	1.88	2.83	1.99	2.09	0.09
FeO	10.64	8.89	9.11	7.48	7.85	8.14	8.04	8.82	7.94	0.00	0.00	1.68
FeO*	12.14	11.17	11.53	9.17	9.77	10.65	9.75	10.51	10.49	1.79	1.88	1.76
MnO	0.22	0.21	0.20	0.18	0.17	0.16	0.13	0.19	0.17	0.01	0.02	0.02
MgO	8.82	6.90	7.73	8.30	8.34	9.37	10.74	11.15	10.04	0.57	0.57	0.98
CaO	11.46	12.72	11.51	14.17	12.78	10.91	12.31	12.43	10.42	2.02	2.12	4.02
Na_2O	2.25	1.28	1.58	1.60	1.36	2.00	1.97	1.56	2.38	4.47	4.70	5.17
K_2O	0.11	0.23	0.25	0.31	0.25	0.08	0.52	0.10	0.48	3.08	2.31	1.05
P_2O_5	0.06	0.06	0.05	0.04	0.04	0.04	0.06	0.06	0.05	0.07	0.08	0.07
Volatiles	1.58	1.5	1.57	1.48	1.57	1.6	1.43	1.53	2.06	0.27	0.10	0.53
Sum	99.74	99.72	99.43	99.11	99.21	99.47	99.29	99.02	99.36	99.23	98.71	99.62
Sc	53.6	49.0	54.8	44.1	44.2	38.7	49.6	52.3	49.7	5.5	8.1	4.6
V	347	283	308	214	237	220	301	297	256	16	13.8	24.1
Cr	106	301	380	444	450	207	521	485	411	5.0	2.6	35.9
Co	53.5	55.1	51.6	51.2	56.1	58.0	70.3	56.6	54.0	17.2	14.7	6.0
Ni	117	150	160	221	222	254	214	221	159	3.6	3.4	12.9
Cu	64.2	89.0	82.7	39.1	90.3	89.5	4.8	82.8	80.8	2.4	8.1	7.3
Zn	91.9	86.0	92.2	74.3	74.8	80.1	40.0	77.3	74.6	40.9	39.8	45.2
Ga	15.7	16.3	15.7	14.2	14.2	14.8	14.8	14.1	15.4	18.2	20.8	23.2
Rb	1.1	7.6	9.1	12.4	10.9	1.2	9.5	2	10.6	82.1	91.4	92.9
Sr	124	111	91	118	150	100	94	109	155	385	303	375
Y	19.6	19.5	19.6	13.6	14.3	14.2	18.1	17.4	17	3	7.8	2.8
Zr	29.7	11.8	12.5	9.4	9.4	15.8	18.4	11.6	16.2	143	117	57.9
Nb	3.1	2	1.9	1.5	1.4	1.1	2.4	2.2	1.7	2.5	4.9	15.4
Cs	0.0	0.3	0.2	0.7	0.8	0.0	0.1	0.0	0.2	1.2	2.6	5.6
Ba	18	56	43	47	25	6	31	20	60	748	446	210
La	3.2	2.2	2.4	1.7	1.6	1.6	3.5	2.5	2.2	34.1	18.9	4.0
Ce	8.4	6.0	6.3	4.5	4.3	4.3	8.0	6.5	6.0	65.0	37.8	8.3
Pr	1.3	1.0	1.0	0.7	0.7	0.7	1.2	1.0	0.9	7.2	4.2	1.0
Nd	6.7	5.3	5.3	3.7	3.7	3.7	6.0	5.6	5.1	24.2	14.9	3.7
Sm	2.2	1.8	1.8	1.4	1.4	1.3	1.9	1.9	1.7	3.3	2.5	0.8
Eu	0.7	0.7	0.7	0.5	0.5	0.6	0.7	0.7	0.6	0.6	0.6	0.3
Gd	3.0	2.7	2.6	1.6	1.7	1.6	2.4	2.3	2.2	3.4	2.6	1.0
Tb	0.5	0.5	0.5	0.3	0.3	0.3	0.5	0.4	0.4	0.2	0.3	0.1
Dy	3.3	3.2	3.1	2.3	2.3	2.3	3.1	2.9	2.8	0.9	1.5	0.6
Ho	0.7	0.7	0.7	0.5	0.5	0.5	0.6	0.6	0.6	0.1	0.3	0.1
Er	1.9	1.9	2.0	1.3	1.4	1.4	1.8	1.7	1.6	0.3	0.7	0.2
Tm	0.3	0.3	0.3	0.2	0.2	0.2	0.3	0.2	0.2	0.0	0.1	0.0
Yb	1.8	1.9	2.0	1.3	1.5	1.4	1.7	1.6	1.6	0.2	0.7	0.2
Lu	0.3	0.3	0.3	0.2	0.2	0.2	0.3	0.3	0.3	0.0	0.1	0.0
Hf	1.0	0.6	0.6	0.4	0.5	0.6	0.7	0.6	0.6	3.8	3.3	1.5
Ta	0.2	0.1	0.1	0.1	0.1	0.1	0.1	0.1	0.1	0.5	1.1	1.9
Pb	1.4	1.5	1.1	1.3	0.8	0.5	0.6	1.3	1.2	9.5	7.6	7.4
Th	0.4	0.2	0.2	0.2	0.2	0.1	0.3	0.3	0.2	10.1	4.2	0.9
U	0.1	0.1	0.1	0.1	0.1	0.0	0.2	0.1	0.0	0.5	0.9	0.4
Total REE	34	28	29	20	20	20	32	28	26	140	85	20

Major elements (in wt%) by XRF at GEUS. Trace elements (in ppm) by ICP-MS at GEUS.
FeO* = total Fe calculated as FeO. Volatiles = loss on ignition corrected for oxygen uptake due to oxidation of iron.

Table 4b. Chemical analyses of various supracrustal rocks

	440910	440931	467503	467404	467408	467417	467420	467423	467433
SiO_2	63.27	69.36	74.26	62.76	61.37	59.87	75.29	49.25	49.94
TiO_2	0.59	0.49	0.03	0.61	0.67	0.64	0.34	0.61	0.78
Al_2O_3	17.61	16.08	14.81	19.09	13.90	16.78	13.01	16.21	15.53
Fe_2O_3	5.19	2.38	0.01	1.17	1.32	1.25	0.51	3.63	1.80
FeO	0.00	0.00	0.37	5.82	6.73	5.38	1.26	6.97	8.34
FeO*	4.67	2.14	0.38	6.87	7.92	6.50	1.72	10.24	9.96
MnO	0.05	0.01	0.00	0.05	0.11	0.15	0.01	0.19	0.16
MgO	2.31	1.03	0.10	2.80	6.41	3.97	0.57	7.70	7.78
CaO	2.26	3.17	2.02	0.75	4.60	3.68	5.62	9.21	10.73
Na_2O	3.84	3.85	4.89	1.60	1.82	2.73	1.05	2.63	1.88
K_2O	3.02	1.79	2.81	3.20	1.46	3.21	0.62	1.63	0.50
P_2O_5	0.13	0.11	0.02	0.03	0.07	0.08	0.05	0.13	0.16
Volatiles	1.00	0.75	0.29	1.64	1.26	1.28	0.90	1.39	1.48
Sum	99.27	99.02	99.62	99.52	99.71	99.01	99.23	99.55	99.06
Sc	18.0	10.2	0.8	17.6	39.3	26.6	7.7	43.8	39.7
V	98.5	38.2	1.7	56.7	208	149	43.5	204	209
Cr	89.1	25.0	0.4	120.0	667	312	66.1	268	318
Co	22.3	17.2	26.9	16.3	44.8	28.4	14.0	51.2	50.7
Ni	32.3	5.2	1.3	54.7	194.0	106.0	34.0	148.0	145.0
Cu	21.9	8.8	5.2	4.8	20.0	26.3	26.9	25.1	34.8
Zn	71.4	38.9	4.4	37.8	89.5	104.5	41.4	81.8	87.4
Ga	20.8	19.6	16.0	25.7	17.5	23.1	15.5	16.3	15.9
Rb	82.7	48.2	58.5	96.9	51.1	197.0	41.6	59.1	8.0
Sr	210	314	402	47	117	177	137	270	288
Y	16.0	6.4	2.4	11.1	15.4	16.7	11.1	17.4	17.0
Zr	134	151	70.8	57.7	82.4	83.1	73.9	38.4	24.0
Nb	5.6	5.6	0.8	8.7	3.3	6.9	2.9	2.3	2.0
Cs	4.1	4.7	0.5	2.0	2.5	8.1	2.7	2.4	0.0
Ba	417	286	591	581	386	377	310	153	97
La	28.2	20.0	7.9	34.5	11.0	9.6	28.3	11.9	13.4
Ce	58.3	40.6	16.1	64.7	29.1	28.5	56.0	29.5	37.5
Pr	6.9	4.4	2.1	7.4	2.9	2.6	6.5	3.8	4.5
Nd	25.3	15.7	7.7	26.4	11.8	10.5	24.5	16.8	19.7
Sm	4.3	2.6	1.8	4.4	2.7	2.5	4.0	3.9	4.4
Eu	1.2	0.7	0.4	0.7	0.7	0.7	1.0	1.2	1.1
Gd	4.5	2.6	1.5	5.0	3.6	2.3	3.9	3.5	3.8
Tb	0.6	0.3	0.2	0.5	0.5	0.4	0.4	0.5	0.5
Dy	3.0	1.4	0.6	2.4	2.8	2.4	2.3	2.9	3.0
Ho	0.6	0.2	0.1	0.4	0.6	0.6	0.4	0.6	0.6
Er	1.6	0.6	0.2	1.1	1.6	1.9	1.1	1.7	1.7
Tm	0.2	0.1	0.0	0.1	0.2	0.3	0.1	0.3	0.3
Yb	1.5	0.5	0.2	0.9	1.5	2.1	0.8	1.6	1.6
Lu	0.2	0.1	0.0	0.1	0.2	0.3	0.1	0.2	0.2
Hf	3.7	3.9	2.8	1.5	2.2	2.2	1.8	1.0	0.8
Ta	0.9	2.6	1.9	0.6	0.3	0.6	0.2	0.1	0.1
Pb	12.7	5.2	11.8	3.7	4.7	9.5	6.1	6.6	4.2
Th	6.2	3.3	4.8	8.5	3.5	6.0	4.2	2.0	2.0
U	1.5	0.9	1.3	0.8	0.9	3.1	0.9	0.7	0.6
Total REE	137	90	39	149	69	65	129	79	92

Major elements (in wt%) by XRF at GEUS. Trace elements (in ppm) by ICP-MS at GEUS.
Volatiles: loss on ignition corrected for oxygen uptake due to oxidation of iron.
FeO*: total Fe calculated as FeO.

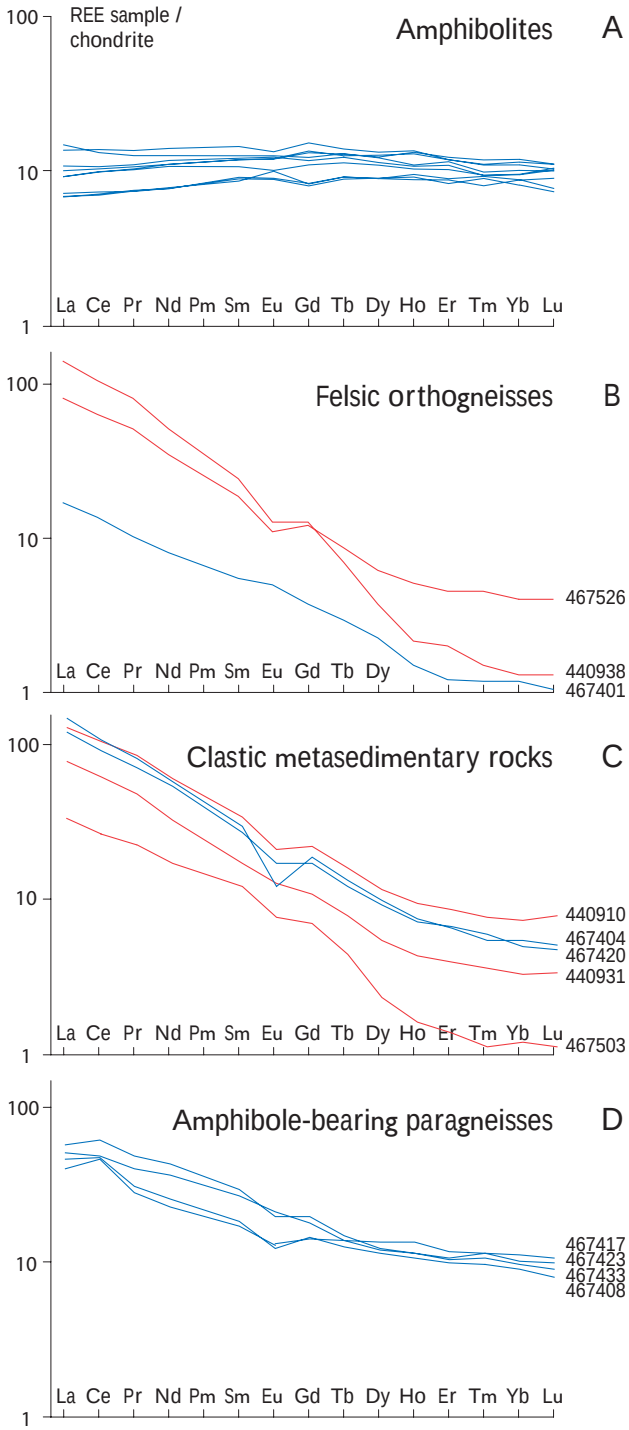

Fig. 8. Chondrite-normalised REE plots. A: amphibolites. B: felsic orthogneiss. C: quartzo-feldspathic metasedimentary rocks. D: mafic metasedimentary rocks. Blue: Samples from the Kangilinaaq region. Red: Samples from the Ikamiut region.

sample 467423. Sample 467408 has an intermediate silica content (61.37 wt% SiO_2), is cummingtonite-bearing, and has high concentrations of MgO (6.41 wt%) and FeO* (7.92 wt%) as well as Cr and N (627 and 186 ppm, respectively). It also has high Ba (405 ppm). The REE curve is almost flat, with ten times chondritic HREE and a weak LREE enrichment (La_N/Lu_N = 5). There is a small positive Ce anomaly in addition to a negative Eu anomaly.

Metasedimentary rocks from the Ikamiut belt

Sample 440910 is the most aluminous (18 wt% Al_2O_3, Table 4), has high REE concentrations, and a fairly steep REE curve with La_N/Lu_N = 15 (Fig. 8C). Samples 440931 and 467503 are more siliceous (69 and 74 wt% SiO_2, respectively) with lower Al, Fe and Mg. Both have lower REE concentrations and slightly steeper REE curves than sample 440910.

Interpretation

The metasedimentary rocks and amphibole-bearing gneisses of supracrustal origin described above from the Ikamiut and Kangilinaaq belts can be divided into two groups based on their geochemical compositions and REE patterns. Five of them, namely all three Ikamiut samples and samples 467404 and 467420 from Kangilinaaq, are typical metasedimentary lithologies with steep REE curves (Fig. 8C). Although they have varying REE concentrations, all five samples have fairly steep REE curves that are comparable to the REE patterns seen in the Kangilinaaq and Ikamiut orthogneisses. The group shows a trend of increasing REE concentrations with decreasing SiO_2 and increasing Al_2O_3, consistent with the general presumption that the REE are preferentially concentrated in the clay fraction of sediments. One exception from this is the siliceous sample 467420 that has REE concentrations comparable to the most aluminous metasediments. Its unusual REE enrichment may be due to high contents of detrital allanite and zircon, as these minerals incorporate high REE concentrations.

The REE curves for the four amphibole-bearing gneisses (467408, 467417, 467423, and 467433; Fig. 8D) have $La_N/Lu_N \sim 5$, showing significantly flatter patterns. These four samples all have high concentrations of mafic minerals and may represent intermediate tuffaceous rocks or mildly chemically altered mafic volcanic rocks. The rather peculiar composition of sample 467408, with high Ni and Cr, suggests that it is a metamorphosed, hydrothermally

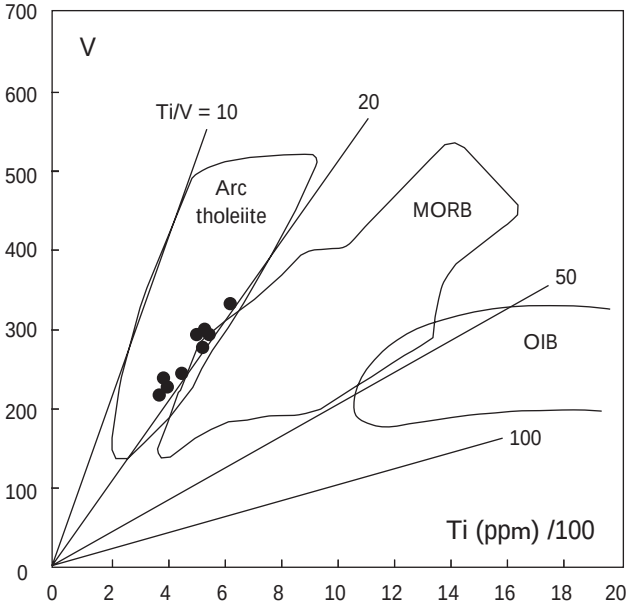

Fig. 9. Ti/V discrimination diagram (Shervais 1982) for nine amphibolite samples from the Kangilinaaq peninsula (Fig. 2B), illustrating their island arc affinities. Note that Ti and V are both immobile elements, considered to be stable during hydrothermal alteration and regional metamorphism (e.g. Nicollet & Andriambololona 1980; Mottl 1983). The partition coefficient of V varies with the oxygen fugacity of the magma, whereas the partition coefficient of Ti remains unchanged.

altered mafic volcanic rock. Alternatively, such high Ni and Cr in a clastic sedimentary precursor would require an abundance of heavy minerals such as garnet and spinel.

Discussion

Regional structures

Both the Ikamiut and Kangilinaaq regions preserve complex tectono-metamorphic histories, and although they show similarities in lithologies and metamorphic grade (amphibolite facies mineral assemblages defining D_1 and D_2 structures) and lie roughly along strike, the large structures are sufficiently different to make a direct correlation between the two regions and their supracrustal belts difficult and dubious. Both regions show evidence for at least two generations of fold structures, with kilometre- to ten kilometre-scale F_2 folds dominating the outcrop pattern. However, there is considerable variation in the typical strike of foliation and plunge of large-scale folds and lineations between the two regions. Furthermore, the aeromagnetic data do not suggest a strong link between the two regions. On the basis of geological mapping and the aeromagnetic data it seems likely that the Kangilinaaq belt forms a synformal fold closure at the south-western tip of the Kangilinaaq peninsula, with little or no westward continuation. We cannot rule out the possibility that there is continuation of this belt across Sydostbugten into the Ikamiut region along an abrupt change in the aeromagnetic response across northern Sydostbugten (boundary O in Fig. 3). This could be interpreted as an extension of the linear aeromagnetic anomaly marking the northern contact of the Qasigiannguit amphibolite sequence with the surrounding orthogneiss, which appears to extend westward to several kilometres north of the Nivaap Paa bay (boundary P in Fig. 3). However, there is no strong field evidence to support this, since no comparable amphibolite sequence occurs on land at Q (Fig. 3). It is possible that this linear aeromagnetic anomaly relates instead to an interpreted granitic body beneath Sydostbugten, represented by outcrop on the south-eastern tip of the Kangilinaaq peninsula, and on the south-west coast of Nivaap Paa.

Magmatism

Geochronological data show that the magmatic precursors to granodioritic orthogneiss from the Ikamiut region were emplaced in the Late Archaean. Sample 440938, with a LA-ICP-MS Pb-Pb zircon age of 2831 ± 23 Ma U-Pb zircon ages of 2820–2810 Ma, is significantly older than sample 467526, which was collected from a nearby locality (LA-ICP-MS Pb-Pb zircon age = 2741 ± 53 Ma). The latter compares well with a homogeneous undeformed granite collected a few kilometres west of the head of Nivaap Paa, which yielded an upper intercept U-Pb zircon age of 2778 +7/–3 Ma (Connelly & Mengel 2000). Similarly, a grey tonalitic orthogneiss sampled close to Aasiaat yielded a U-Pb concordia age of 2727 +36/–22 Ma and consistent Pb-Pb and Rb-Sr whole-rock ages of 2759 +87/–92 Ma and 2752 ± 656 Ma respectively (Kalsbeek *et al.* 1987).

Available data on emplacement ages of the precursors to the tonalitic orthogneiss in the Kangilinaaq region suggest these may be slightly older than those in the Ikamiut region. Kalsbeek & Nutman (1996) reported ion probe data for a few zircon grains from a granodioritic to granitic orthogneiss in the Kangilinaaq area, which gave an emplacement age between 2900 and 2750 Ma. Keiding (2004) presented LA-ICP-MS $^{207}Pb/^{206}Pb$ zircon age data for a tonalitic orthogneiss of 2818 ± 1 Ma, interpreted as an igneous crystallisation age.

Sedimentation

Deposition of the sedimentary precursors to the Ikamiut and Kangilinaaq belts likely occurred in the Neoarchaean, as indicated by the metamorphic ages of *c*. 2800–2700 Ma of zircon from both belts. The age of the Kangilinaaq belt is further constrained by the 2723 ± 15 Ma emplacement age of a two-mica granite, which cross-cuts pelitic metasedimentary rocks of this belt on the south shore of Kangersuneq fjord (Thrane & Connelly 2006, this volume). As regards the Ikamiut belt, its detrital zircon ages do not preclude deposition after the Archaean. Neoarchaean metamorphic rims have been observed on some detrital grains, but these might have formed already during metamorphism of the source and survived during erosion and deposition. However, we consider this possibility unlikely. A Neoarchaean depositional age is furthermore in agreement with the Rb-Sr isotopic data for 12 metasedimentary samples from Ikamiut reported by Kalsbeek & Taylor (1999), which likewise show that their source was Archaean. Finally, the Ikamiut belt has experienced a more complex structural history than the Naternaq supracrustal belt of Palaeoproterozoic age to its south (Østergaard *et al*. 2002; Garde 2004; Thrane & Connelly 2006, this volume). This likewise points to an Archaean age of the Ikamiut belt.

The depositional sources themselves are constrained by detrital zircon populations. The detrital age spectrum for zircon grains (with igneous zonation) from metasedimentary sample 440910 from the Ikamiut region forms a tightly clustered peak at *c*. 2800 Ma, consistent with the age of the older tonalitic orthogneiss in this area. Furthermore, the steep REE pattern of this sample mimics that of the granodioritic to tonalitic orthogneiss that dominates the region. Thus the sedimentary precursor to this rock was probably derived locally from (and possibly deposited onto) the igneous precursor to the Neoarchaean orthogneiss basement. This requires a tectonic environment conducive to rapid erosion of the precursor to the source orthogneiss shortly after its emplacement at *c*. 2800 Ma.

Similarly, a metasedimentary rock from the Kangilinaaq region contains Archaean detrital zircon, with a strong peak at *c*. 2800 Ma (Thrane & Connelly 2006, this volume, $^{207}Pb/^{206}Pb$ zircon). However, there is also evidence for a significant older component, not recognised in metasedimentary rocks from the Ikamiut region: Keiding (2004) reported detrital zircon ages for two metasedimentary samples from the Kangilinaaq region with grains as old as 3600 Ma, and down to 2500 Ma, although the youngest grains (< 2800 Ma) were suspected of having suffered lead loss. Both samples show a large spread of ages, but neither has a significant Neoarchaean component at *c*. 2800 Ma. These data contrast with those of sample 440910 from the Ikamiut region, which has a tightly clustered detrital zircon population at *c*. 2800 Ma. This suggests that at least some of the Kangilinaaq metasedimentary rocks were derived from different, older, and distal source rocks: the older (> 2900 Ma) component may be derived from a presently unexposed region within the Nagssugtoqidian orogen or possibly from the lesser-known craton to the north (Keiding 2004).

A difference in the depositional sources of the Ikamiut and Kangilinaaq belts is also apparent from the geochemical data. The metasedimentary rocks form two groups based on their REE patterns. The first group (three Ikamiut and two Kangilinaaq samples) shows steep REE curves (Fig. 8C), interpreted as indicative of derivation from a felsic source, based on their similarity with REE patterns seen in the Kangilinaaq and Ikamiut orthogneisses. The second group (four Kangilinaaq samples, Fig. 8D) shows flatter patterns, consistent with derivation from a bimodal source, i.e. detritus of both felsic (steep REE patterns) and mafic (flat REE patterns) igneous rocks. The precursors to the amphibole-bearing gneisses are interpreted as volcaniclastic material that may have been mixed with clastic material during deposition or by tectonic interleaving. Given the intensity of deformation and paucity of information on the depositional environment(s) we consider it imprudent to establish a single stratigraphic-structural interpretation. In view of the different dominant lithologies of the Qasigiannguit amphibolite and the remainder of the Kangilinaaq belt, it would be interesting to investigate further whether they represent the same or different settings. The geochemistry of their amphibolite samples fall within the same range, but no metasedimentary rocks associated with the Qasigiannguit amphibolite have been analysed, and these may be important for identifying links between the latter unit and the Kangilinaaq belt.

Metamorphism

Age data for metamorphic zircon from orthogneiss and metasedimentary samples from the Ikamiut region indicate an important Neoarchaean thermal event. Two analyses of metamorphic rims from the 2831 ± 23 Ma orthogneiss 440938 yield ages of 2761 ± 10 Ma and 2754 ± 5 Ma, within error the same as the 2741 ± 53 Ma emplacement age of sample 467526 (Fig. 7). This may suggest that continued synkinematic emplacement of Neoarchaean granitoids at *c*. 2760–2700 Ma resulted in metamorphism

of slightly older (*c*. 2800 Ma) crust. This is also supported by U-Pb zircon data from the metasedimentary sample 440910. The six SIMS ages of metamorphic rims fall in two ranges, 2741 ± 9 Ma and 2696 ± 6 Ma, and similar young ages were identified in the LA-ICP-MS data (Fig. 7). These ages probably relate to the growth of S_1 garnet, biotite, plagioclase, quartz, minor sillimanite and K-feldspar in this and other metasedimentary rocks, indicative of amphibolite facies conditions only shortly after deposition, and predating regional F_2 folding. Neoarchaean metamorphism has also been recognised from zircon age data in the Kangilinaaq region. Keiding (2004) reported *c*. 2800 and 2760 Ma LA-ICP-MS ages of zircon rims and discrete grains, interpreted as metamorphic in origin, in a 2818 ± 1 Ma tonalitic orthogneiss. These ages correlate reasonably well with 2810–2720 Ma metamorphic U-Pb zircon and monazite ages in 2870–2810 Ma orthogneisses from throughout the Nagssugtoqidian orogen (Connelly & Mengel 2000).

It is likely that Neoarchaean amphibolite facies metamorphism in the Ikamiut and Kangilinaaq regions was the product of tectonism along a convergent margin (see also Connelly & Mengel 2000) on the basis of (1) the tonalitic to granodioritic composition of the Neoarchaean regional orthogneisses, (2) the apparent island arc geochemical character of amphibolites of the Kangilinaaq belt, (3) differences in the ages of sediment sources in the two supracrustal belts, and (4) the rapidity of the cycle of magmatism, erosion, sedimentation, and metamorphism.

Proterozoic zircon ages are known from the Kangilinaaq region. Keiding (2004) reported 1920–1820 Ma LA-ICP-MS ages of zircon rims and discrete grains in Archaean tonalitic orthogneisses, and also reported weighted mean age of 1919 ± 11 Ma from three rims of detrital grains in a metasedimentary rock from the Kangilinaaq belt. Thrane & Connelly (2006, this volume) report metamorphic ages of *c*. 1850 Ma for a metasedimentary rock collected on the south shore of Kangersuneq fjord, attributed to the peak of regional Nagssugtoqidian metamorphism. Given the consistency of ENE-trending D_2 structures in the Kangilinaaq and Ikamiut regions with ENE-trending Palaeoproterozoic structures throughout the orogen, these are interpreted as the product of the *c*. 1850 Ma Nagssugtoqidian orogenesis. The significance of the slightly older, *c*. 1920 Ma metamorphic age is not clear, but may indicate that part of this region experienced a thermal event prior to the main regional Nagssugtoqidian orogenesis.

By contrast, no significant indications of Palaeoproterozoic resetting are found in our Ikamiut data. The slightly discordant zircon data in sample 440938 suggest some Pb loss in this sample, although the timing is not clear. Similarly, three titanite U-Pb analyses of 2778 +7/–3 Ma reported by Connelly & Mengel (2000) from a homogeneous, undeformed granite plot on a discordia line between 2789 ± 100 and 1775 ± 10 Ma. This indicates that Palaeoproterozoic metamorphic temperatures were too low to completely reset titanite in this region. Likewise, no indication of U-Pb resetting in zircon was found in the 2727 +36/–22 Ma age from a tonalitic gneiss reported by Kalsbeek *et al*. (1987). This contrasts with zircon U-Pb analyses of samples from the Nordre Strømfjord region in the core of the Nagssugtoqidian orogen, which experienced significant Pb-loss at *c*. 1850 Ma (Kalsbeek *et al*. 1987).

Conclusions

New mapping, geochemical, geochronological and geophysical studies of two supracrustal belts from Sydostbugten, southern Disko Bugt region, West Greenland, shed light on the Neoarchaean tectonic evolution of the northern Nagssugtoqidian basement. The Kangilinaaq belt was deposited at *c*. 2800 Ma, whereas the deposition of the Ikamiut belt may postdate *c*. 2740 Ma. The geochemical signatures of the majority of metasedimentary samples from the Kangilinaaq region show REE patterns indicative of mixed felsic and mafic sources with distal Meso- and Palaeoarchaean components that are not currently known *in situ* in this part of West Greenland. Island-arc geochemical affinities of intercalated amphibolites are consistent with deposition in an arc setting. In contrast, the Ikamiut belt was sourced locally from, and deposited onto or proximal to the igneous precursors of Neoarchaean granodioritic to tonalitic orthogneisses. This is constrained by (1) the similarity in REE signatures of metasedimentary rocks and local orthogneisses and (2) the zircon emplacement ages of orthogneisses (*c*. 2820–2810 Ma; 2831 ± 23 Ma; 2741 ± 53 Ma) and detrital zircons in metasediment (2779 ± 18 Ma).

Zircon U-Pb data and $S_{1–2}$ sillimanite-bearing mineral assemblages (this study and existing data) indicate that *c*. 2800–2700 Ma amphibolite facies metamorphism affected both regions, shortly after the emplacement of the regional orthogneiss precursors and deposition of the supracrustal rocks. The rather rapid cycle of magmatic emplacement, island arc volcanism, erosion and sedimentation, and subsequent amphibolite facies metamorphism is consistent with Neoarchaean convergent tectonism at the northern margin of the present Nagssugtoqidian orogen.

Subsequently, both regions underwent Palaeoproterozoic regional deformation and lower amphibolite facies

metamorphism at *c.* 1850 Ma during the Nagssugtoqidian orogenesis, the effects of which control outcrop patterns in both areas. In the Ikamiut region, the supracrustal belt defines a broad, shallowly W-plunging antiformal structure with associated kilometre-scale parasitic F_2 folds. S_1 fabrics are folded into metre- to kilometre-scale F_2 folds and variably transposed into ENE-striking, steeply dipping S_2 fabrics and shallow W-plunging mineral lineations defined by biotite and muscovite.

In the Kangilinaaq region, the supracrustal belt defines a broad, NE-plunging F_2 fold structure. A pervasive, NE-striking, moderately dipping S_2 fabric, defined by medium- to coarse-grained garnet-hornblende-biotite-sillimanite-bearing assemblages in pelitic rocks, is folded into F_3 folds, and attests to amphibolite facies metamorphic conditions during deformation. Lack of Palaeoproterozoic resetting of the zircon U-Pb isotopic system in the Ikamiut region, cf. the Kangilinaaq region, suggests that temperatures were relatively lower in the former region during the Nagssugtoqidian orogenesis.

Acknowledgements

Mads Sylvest Christensen, Jane Gilotti, Christian Knudsen, Stanislaw Mazur, Mac Persson, Sandra Piazolo and Thomas V. Rasmussen contributed to field work in 2002–2003 reported here and part of the GEUS project *Archaean and Proterozoic crustal evolution in the Aasiaat region, central West Greenland.* Dirk Frei, Mark T. Hutchison, Lev Ilyinsky, Jørgen Kystol, Ingerlise Nørgaard, Thomas V. Rasmussen, Mikkel Vognsen, and Martin Whitehouse provided support and assistance in sample preparation and collection of analytical data. The Nordsim laboratory is funded and operated under agreement between the research funding agencies of Denmark, Norway, and Sweden, GTK, Finland, and Naturhistoriska Riksmuseet, Sweden; this is Nordsim contribution no. 164. Clark Friend, Lotte Melchoir Larsen and an anonymous reviewer are thanked for critical reviews.

References

Connelly, J.N. & Mengel, F.C. 2000: Evolution of Archean components in the Paleoproterozoic Nagssugtoqidian orogen, West Greenland. Geological Society of America Bulletin 112, 747–763.

Connelly, J.N., van Gool, J.A.M. & Mengel, F.C. 2000: Temporal evolution of a deeply eroded orogen: the Nagssugtoqidian orogen, West Greenland. Canadian Journal of Earth Sciences 37, 1121–1142.

Garde, A.A. 2004: Geological map of Greenland, 1:100 000, Kangaatsiaq, 68 V.1 Syd. Copenhagen: Geological Survey of Denmark and Greenland.

Garde, A.A. in press: Geological map of Greenland, 1:100 000, Ikamiut, 68 V.1 Nord. Copenhagen: Geological Survey of Denmark and Greenland.

Garde, A.A. & Steenfelt, A. 1999: Precambrian geology of Nuussuaq and the area north-east of Disko Bugt, West Greenland. Geology of Greenland Survey Bulletin 181, 6–40.

Garde, A.A., Christiansen, M.S., Hollis, J.A., Mazur, S. & van Gool, J.A.M. 2004: Low-pressure metamorphism during Archaean crustal growth: a low-strain zone in the northern Nagssugtoqidian orogen, West Greenland. Geological Survey of Denmark and Greenland Bulletin 4, 73–76.

Henderson, G. 1969: The Precambrian rocks of the Egedesminde–Christianshåb area (sheets 68V.1 and 68V.2). Rapport Grønlands Geologiske Undersøgelse 23, 1–37.

Hollis, J.A., Garde, A.A., van Gool, J.A.M. & Thrane K. 2004: Polymetamorphism in the northern Nagssugtoqidian orogen: a review and presentation of recent data. Danmarks og Grønlands Geologiske Undersøgelse Rapport 2004/17, 25–27.

Jacobsen, B.H. 1987: A case for upward continuation as a standard separation filter for potential-field maps. Geophysics 52, 1138–1148.

Kalsbeek, F. & Nutman A.P. 1996: Anatomy of the Early Proterozoic Nagssugtoqidian orogen, West Greenland, explored by reconnaissance SHRIMP U-Pb zircon dating. Geology 24, 515–518.

Kalsbeek, F. & Taylor, P.N. 1999: Review of isotope data for Precambrian rocks from the Disko Bugt region, West Greenland. Geology of Greenland Survey Bulletin 181, 41–47.

Kalsbeek, F., Pidgeon, R.T. & Taylor, P.N. 1987: Nagssugtoqidian mobile belt of West Greenland: a cryptic 1850 Ma suture between two Archaean continents – chemical and isotopic evidence. Earth and Planetary Science Letters 85, 365–385.

Keiding, M. 2004: Petrologiske og geokronologiske unders¿gelser af prækambriske bjergarter fra Kangilinaaq, Vestgrønland, 70 pp. Unpublished Master thesis, Københavns Universitet, Danmark.

Kystol, J. & Larsen, L.M. 1999: Analytical procedures in the Rock Geochemical Laboratory of the Geological Survey of Denmark and Greenland. Geology of Greenland Survey Bulletin 184, 59–62.

Ludwig, K.R. 2000: Isoplot/Ex version 2.2: a geochronological toolkit for Microsoft Excel. Berkeley: Berkeley Geochronology Center.

Mazur, S., Piazolo, S. & Alsop, G.I. 2006: Structural analysis of the northern Nagssugtoqidian orogen, West Greenland: an example of complex tectonic patterns in reworked high-grade metamorphic terrains. In: Garde, A.A. & Kalsbeek, F. (eds): Precambrian crustal evolution and Cretaceous–Palaeogene faulting in West Greenland. Geological Survey of Denmark and Greenland Bulletin 11, 163–178 (this volume).

Mottl, M.J. 1983: Metabasalts, axial hot springs, and the structure of hydrothermal systems at mid-ocean ridges. Geological Society of America Bulletin 94, 161–180.

Nicollet, C. & Andriambololona, D.R. 1980: Distribution of transition elements in crustal metabasic igneous rocks. Chemical Geology 28, 79–90.

Nielsen, B.M. & Rasmussen, T.M. 2004: Mineral resources of the Precambrian shield of central West Greenland (66° to 70°15′N). Part

3. Implications of potential field data for the tectonic framework. Danmarks og Grønlands Geologiske Undersøgelse Rapport 2004/21, 165 pp.

Noe-Nygaard, A. & Ramberg, H. 1961: Geological reconnaissance map of the country between latitudes 69°N and 63°45′N, West Greenland. Meddelelser om Grønland 123, 1–9.

Østergaard, C., Garde, A.A., Nygaard, J., Blomsterberg, J., Nielsen, B.M., Stendal, H. & Thomas, C.W. 2002: The Precambrian supracrustal rocks in the Naternaq (Lersletten) and Ikamiut areas, central West Greenland. Geology of Greenland Survey Bulletin 191, 24–32.

Pearce, N.J.G., Perkins, W.T., Westgate, J.A., Gorton, M.P., Jackson, S.E., Neal., C.R. & Cheney, S.P. 1997: A compilation of new and published major and trace element data for NIST SRM 610 and NIST SRM 612 glass reference material. Geostandards Newsletter 21, 115–144.

Piazolo, S., Alsop, G.I., Nielsen, B.M. & van Gool, J.A.M., 2004: The application of GIS to unravel patterns of deformation in high grade terrains: a case study of indentor tectonics from West Greenland. In Alsop, G.I. & Holdsworth, R.E. (eds): Flow processes in faults and shear zones. Geological Society Special Publication (London) 224, 63–78.

Shervais, J.W. 1982: Ti-V plots and the petrogenesis of modern and ophiolitic lavas. Earth and Planetary Science Letters 59, 101–118.

Taylor, P.N. & Kalsbeek, F. 1990: Dating the metamorphism of Precambrian marbles: examples from Proterozoic mobile belts in Greenland. Chemical Geology 86, 21–28.

Taylor, S.R. & McLennan, S.M. 1985: The continental crust: its composition and evolution, 312 pp. Oxford: Blackwell Scientific Publications.

Thorning, L. 1993: Project AEROMAG-92: a new high resolution aeromagnetic survey of the Lersletten area, central West Greenland (68°15′ to 68°55′N, 50°25′ to 53°35′W). Open File Series Grønlands Geologiske Undersøgelse 93/2, 36 pp.

Thrane, K. & Connelly, J.N. 2006: Zircon geochronology from the Kangaatsiaq–Qasigiannguit region, the northern part of the 1.9–1.8 Ga Nagssugtoqidian orogen, West Greenland. In: Garde, A.A. & Kalsbeek, F. (eds): Precambrian crustal evolution and Cretaceous–Palaeogene faulting in West Greenland. Geological Survey of Denmark and Greenland Bulletin 11, 87–99 (this volume).

van Gool, J.A.M. 2005: Geological map of Greenland, 1:100 000, Kangersuneq, 68 V.2 Syd. Copenhagen: Geological Survey of Denmark and Greenland.

van Gool, J.A.M., Connelly, J.N., Marker, M. & Mengel, F.C. 2002a: The Nagssugtoqidian orogen of West Greenland: tectonic evolution and regional correlations from a West Greenland perspective. Canadian Journal of Earth Sciences 39, 665–686.

van Gool, J.A.M. *et al.* 2002b: Precambrian geology of the northern Nagssugtoqidian orogen, West Greenland: mapping in the Kangaatsiaq area. Geology of Greenland Survey Bulletin 191, 13–23.

Whitehouse, M.J., Claesson, S., Sunde, T. & Vestin, J. 1997: Ion microprobe U-Pb zircon geochronology and correlation of Archaean gneisses from the Lewisian Complex of Gruinard Bay, northwestern Scotland. Geochimica et Cosmochimica Acta 61/20, 4429–4438.

Wiedenbeck, M., Alle, P., Corfu, F., Griffin, W.L., Meier, M., Oberli, F., von Quadt, A., Roddick, J.C. & Spiegel, W. 1995: Three natural zircon standards for U-Th-Pb, Lu-Hf, trace element and REE analyses. Geostandards Newsletter 19/1, 1–23.

Manuscript received 4 October 2004; revision accepted 15 February 2006